# Heat and Buoyancy Budgets and Mixing Rates in the Upper Thermocline of the Indian and Global Oceans

HUAI-MIN ZHANG* AND LYNNE D. TALLEY

*Scripps Institution of Oceanography, University of California, San Diego, La Jolla, California*

(Manuscript received 17 April 1997, in final form 16 December 1997)

ABSTRACT

Diapycnal and diathermal diffusivity values in the upper thermocline are estimated from buoyancy and heat budgets for water volumes bounded by isopycnals and isotherms, the air–sea interface, and coastline where applicable. Comprehensive analysis is given to the Indian Ocean, with an extended global general description.

The Indian Ocean gains buoyancy in the north (especially in the northeast) and loses buoyancy in the subtropical south. Freshest and least-dense water appears in the Bay of Bengal and isopycnals outcrop southwestward from there and then southward. Computation of diapycnal diffusivity ($K_\rho$) starts from the Bay of Bengal, expanding southwestward and southward and with depth. As isopycnals extend equatorward from the northeast and with increasing depth, $K_\rho$ remains at about 1.3 cm$^2$ s$^{-1}$ for 20.2 $\sigma_\theta$ (Bay of Bengal) to 22.0 $\sigma_\theta$ (northeast Indian Ocean). Farther south (poleward) and at greater depth, $K_\rho$ decreases from 0.9 cm$^2$ s$^{-1}$ for 23.0 $\sigma_\theta$ (north of 20°S) to 0.5 cm$^2$ s$^{-1}$ for 25.0 $\sigma_\theta$ (north of 35°S). Isotherms outcrop poleward from the equator. Diathermal diffusivity values computed from the heat budget are large at the equator and near the surface (4.0 cm$^2$ s$^{-1}$ for 28.5°C isotherm) but decrease rapidly poleward and with depth (1.3 cm$^2$ s$^{-1}$ for 27.0°C). This indicates stronger mixing either near the equator or the surface, or a possible component in the diathermal direction of the larger isopycnal diffusivity, as isotherms do not follow isopycnals in the upper Indian Ocean north of 10°S. For the 21.0°C isotherm, which closely follows isopycnal 25.0 $\sigma_\theta$, the heat budget yields a $K_\theta$ again of 0.5 cm$^2$ s$^{-1}$, the value of the diapycnal diffusivity.

For the Indian–Pacific system, $K_\rho$ decreases from 1.3 cm$^2$ s$^{-1}$ for 22.0 $\sigma_\theta$ (the warm pool water, depth ~60 m) to 0.9 cm$^2$ s$^{-1}$ for 23.0 $\sigma_\theta$ (the tropical water between 20°N and 20°S, depth ~100 m), and to 0.1 cm$^2$ s$^{-1}$ for 25.0 $\sigma_\theta$ (40°N–40°S, depth ~170 m). In the eastern tropical Pacific, $K_\rho$ = 1.1 cm$^2$ s$^{-1}$ for 21.5 $\sigma_\theta$ (depth ~25 m) while $K_\rho$ = 0.6 cm$^2$ s$^{-1}$ for 22.0 $\sigma_\theta$ (depth ~35 m). In the Atlantic, $K_\rho$ = 0.6 cm$^2$ s$^{-1}$ for 24.0 $\sigma_\theta$ between 20°N and 15°S (depth ~80 m), and 0.2 cm$^2$ s$^{-1}$ for 25.0 $\sigma_\theta$ between 30°N and 35°S (depth ~120 m). For the water volume bounded by 25.5 $\sigma_\theta$ farther south and north (50°N–40°S), air–sea buoyancy gain in the Tropics is about the size of the buoyancy loss in the subtropics, and the near-zero net flux may not have significance compared to the errors in the data. For 27.5 $\sigma_\theta$, which encompasses the large region from about 65°N to the Antarctic (with midocean average depth of 400 m), $K_\rho$ is 0.2 cm$^2$ s$^{-1}$. The results indicate that mixing strength generally decreases poleward and with depth in the upper ocean.

## 1. Introduction

Theoretical and modeling efforts have shown that diapycnal mixing is central to the dynamics of the ocean thermocline and the deep ocean (e.g., Stommel and Arons 1960; Welander 1971; Tziperman 1986). How to accurately parameterize the flux caused by eddy activities is one of the major problems in the numerical modeling of the climate (coupled atmosphere–ocean) system because of the lack of knowledge of mixing rates in the ocean. (e.g., Gargett and Holloway 1992.) The limited available estimates for diapycnal eddy diffusivity range from $O(0.1)$ to $O(100)$ cm$^2$ s$^{-1}$ and depend on location as well as the estimation methods. Bulk diapycnal diffusivities estimated from diagnostic models for large-scale water property distributions (mass, heat, salt, and other tracer balances) are of $O(1)$ cm$^2$ s$^{-1}$ (e.g., Munk 1966; Hogg 1987; Spitzer and Jenkins 1987; Zhang and Hogg 1992), while those inferred from direct microstructure measurements are of $O(0.1)$ cm$^2$ s$^{-1}$ in the ocean interior (e.g., Gregg 1987; Ledwell et al. 1993; Toole et al. 1994; Sherman and Davis 1995). Microstructure measurements and deep mass and heat balances indicate that much larger diffusivities are likely at boundaries (Toole et al. 1994; Ledwell and Hickey 1995; Ledwell and Bratkovich 1995; Whitehead and Worthington 1982; Hogg et al. 1982; Roemmich et al.

* Current affiliation: Graduate School of Oceanography, University of Rhode Island, Narragansett, Rhode Island.

*Corresponding author address:* Dr. Huai-Min Zhang, Department of Physical Oceanography, Graduate School of Oceanography, University of Rhode Island, 215 South Ferry Road, Narragansett, RI 02882-1197.
E-mail: zhang@nippawas.gso.uri.edu

1996; Polzin et al. 1997), probably due to internal wave breaking (Eriksen 1985; Gargett 1990; Gregg and Kunze 1991; Moum et al. 1992; Duda and Jacobs 1995). Enlarged diffusivity values in the surface layer and near the equator are also presented (Chereskin et al. 1986; Hebert et al. 1991; de Szoeke 1995). In the present work we extend the previous efforts determining the diffusivity values and fill some gaps in the literature. We will see that the diapycnal and diathermal diffusivity values vary between $O(1)$ and $O(0.1)$ cm$^2$ s$^{-1}$ in the upper waters of the oceans.

Our calculation of average eddy diffusivities begins with the Indian Ocean because of its unique isopycnal distribution patterns, which are determined by strong heating and freshwater input in the northeast. We could equally well have started in another tropical region but chose to concentrate our most comprehensive analysis on the Indian Ocean. In terms of the climatological annual mean air–sea surface heat and freshwater fluxes (e.g., Baumgartner and Reichel 1975; Hastenrath and Lamb 1980; Hsiung 1985; da Silva et al. 1994), the Indian Ocean can be divided into three regions (Fig. 2). In the northeast and central region (including the Bay of Bengal), the ocean gains both heat and freshwater and thus buoyancy from the atmosphere and from the intensive river runoff. The surface water is characterized by low salinity and high temperature. The net annual-mean buoyancy gain results in an annual net production of the least dense water. On the other hand, in the subtropical region (say, 15°S–45°S), the regime is just the opposite: the ocean loses both heat and freshwater and thus buoyancy. The surface water in this band features high salinity. The net annual-mean buoyancy loss results in an annual net production of denser water. In the third, northwest region including the Arabian Sea, the regime is a mixture of the above two. The ocean gains heat but loses freshwater due to the excess evaporation over precipitation. These two processes have opposite effects on the buoyancy change, and the former dominates the latter, resulting in a net buoyancy gain. In contrast to the warm and fresher water in the Bay of Bengal, the Arabian Sea has saltier and cooler surface water. Annually, this area features a production of salty water due to evaporation and a production of less dense water due to the dominant surface heating.

The different regimes of air–sea flux result in the formation of different near-surface water masses. How (by mixing and/or advection?) and how much of the water masses are exported from the surface to depth and from one region to another are unclear, and our understanding of the broad thermohaline circulation in the Indian Ocean is incomplete. The strength of the thermohaline overturning varies in previous studies. Based on sparsely sampled zonal hydrographic sections near 32°S and repeated observations of the Agulhas Current off Durban, Toole and Raymer (1985) estimated a weak net northward mass transport at depth. Assimilating a climatological dataset into a GCM, Lee and Marotzke (1996) found vigorous meridional overturning only in the upper 1000 m; little net deep inflow was found entering the Indian Ocean from the south. A GCM simulation of the global ocean circulation by Semtner and Chervin (1992) also showed little net northward transport at depth in the Indian Ocean. Fu's (1986) and Macdonald's (1995) box inverse models, however, estimated a moderate net northward transport below 2000 m. Also, Toole and Warren (1993) derived a northward geostrophic transport of 27 Sv (Sv $\equiv 10^6$ m$^3$ s$^{-1}$) below 2000 m across 32°S using a transoceanic hydrographic section, and Robbins and Toole (1996) revised this number to 11.9 Sv by adding the silica budget. The relative importance of wind stress forcing versus buoyancy forcing in driving the annual-mean thermohaline circulation is also unknown. Motivated by the strong differential heating over the Indian Ocean discussed above, Warren (1994) formulated a simple two-layer model showing that the deep upwelling varies with the square root of the heat-flux differential. As a result a strong meridional surface heat-flux differential could drive a vigorous deep overturning.

Concentrating first on the Indian Ocean after the methodology (section 2), we analyze the water-mass formation rates at the sea surface and the strength of mixing in the upper ocean from climatological atlases of air–sea flux (da Silva et al. 1994) and hydrography (Levitus et al. 1994) (section 3). Diapycnal and diathermal eddy fluxes and thus average eddy diffusivity values are computed from the buoyancy and heat budgets for water volumes bounded by various isopycnals and isotherms, the air–sea interface, and coastline (sections 4 and 5). Geographical distribution of the average diffusivity values is then discussed. The roles of river runoff and the Indonesian Throughflow are specifically examined. Computations are then extended to other oceans in section 6, followed by discussions and conclusions in section 7.

## 2. Method

The analysis follows the methodology of Walin (1982), Niiler and Stevenson (1982), Speer and Tziperman (1992), Speer et al. (1995), and Garrett et al. (1995). Walin (1982) presented relations between differential heating, diffusive heat flux, and surface advection. Niiler and Stevenson (1982) pointed out that the air–sea heat flux over the warm water pools in the tropical Atlantic and Pacific is principally balanced by turbulent diffusion of heat out of the warm pools. Speer and Tziperman (1992) and Speer et al. (1995) computed the water-mass formation rates in terms of surface density classes. Garrett at al. (1995) further discussed the relationship between water mass formation and the surface buoyancy flux.

Assuming a steady state for a climatological annual mean dataset, it is possible to estimate the eddy fluxes across an isopycnal surface from the air–sea heat and

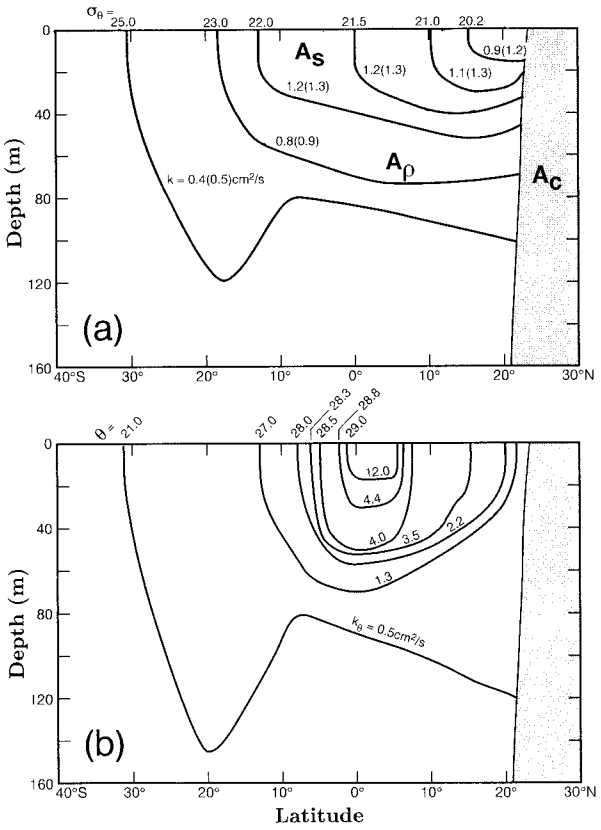


FIG. 1. Diapycnal (a) and diathermal (b) diffusivities in the Indian Ocean estimated from the buoyancy and heat budgets for water volumes bounded by isopycnal/isotherm surfaces ($A_\rho/A_\theta$), air–sea interface $A_s$, and coastline $A_c$.

freshwater (thus density/buoyancy) fluxes through various conservation equations (Niiler and Stevenson 1982; Hogg et al. 1982; Whitehead and Worthington 1982). If the diapycnal density gradients can also be obtained from a hydrographic dataset, the diapycnal eddy diffusivity values can be computed from the conventional parameterization of the eddy flux, as outlined below.

For a climatological annual mean dataset, the density conservation and continuity equations, including the eddy flux terms, can be written as

$$\nabla\cdot(\mathbf{V}\rho) + \nabla\cdot\langle\mathbf{V}'\rho'\rangle = Q_\rho \tag{2.1}$$

$$\nabla\cdot\mathbf{V} = 0, \tag{2.2}$$

where $\mathbf{V}$ is the 3D velocity and $Q_\rho$ the source/sink term for the density $\rho$ (or buoyancy). The quantities without primes are the annual means in this paper, and the primes are the fluctuations from the annual means. The eddy flux term in angle brackets represents an ensemble mean in theory, but in practice is replaced by a limited time mean. Integrating the above equations over the surfaces of an enclosed water bounded by the isopycnal surface $A_\rho$, the sea surface $A_s$, and the coast area $A_c$ (Fig. 1a) yields

$$\int_{A_\rho} V_n\rho\, dA + \int_{A_\rho}\langle V_n'\rho'\rangle\, dA = \int_{A_s} Q_\rho\, dA \tag{2.3}$$

$$\int_{A_\rho} V_n\, dA = 0, \tag{2.4}$$

assuming no water exchange between the ocean and the ocean bottom. Here $V_n$ is the velocity normal to the surface element $dA$. Along an isopycnal surface $A_\rho$, $\rho$ is constant, so the first term in Eq. (2.3) vanishes by using Eq. (2.4). This states that for the steady state, the annual mean circulation brings no buoyancy divergence through the isopycnal surfaces. However, river runoff and the Indonesian Throughflow produce buoyancy convergence since the inflow water is lighter than the outflow water (cf. sections 4a and 4b for numerics). Taking into account this effect, Eq. (2.3) simplifies to

$$\int_{A_\rho}\langle V_n'\rho'\rangle\, dA = \int_{A_s} Q_\rho\, dA + \Delta\int_{A_\rho} V_n\rho\, dA, \tag{2.5}$$

where the last term represents the convergence associated with river runoff and the throughflow. Equation (2.5) states that the density gain/loss through the air–sea surface, the runoff, and the throughflow must be carried out of/into the water volume by the eddy flux across the isopycnal surface (bottom of the water volume) to maintain the annual mean steady state.

Equation (2.5) gives the integral effect of the eddy flux over the whole isopycnal surface that bounds the water volume. Eddy flux is generally a function of space. Without further information, the distribution of eddy flux over the isopycnal cannot be assessed by the above method. Instead, we can compute only an averaged eddy flux (per unit area) as

$$\overline{\langle V_n'\rho'\rangle} = \frac{\displaystyle\int_{A_\rho}\langle V_n'\rho'\rangle\, dA}{\displaystyle\int_{A_\rho} dA}, \tag{2.6}$$

where the overbar represents the average (mean) over the whole isopycnal surface $A_\rho$.

The density eddy flux is an accumulated effect of the correlation between the fluctuations of velocity and density. If this process is parameterized as a diapycnal diffusive process, we can compute an average eddy diffusivity from the relation

$$\overline{\langle V_n'\rho'\rangle} = -K\overline{\frac{\partial\rho}{\partial z}}, \tag{2.7}$$

where $\overline{\partial\rho/\partial z}$ is the mean diapycnal density gradient averaged over the isopycnal surface.

The calculations are mainly relegated to the upper thermocline because of the requirement of closed isopycnals. Consequently, part of each isopycnal surface

is in the surface mixed layer. Effectively, the whole bounding isopycnal surface can be divided into vertical and lateral portions. The horizontal eddy flux through the vertical section, whose depth is determined by the mixed layer depth, can be parameterized as $K_H\overline{\partial\rho/\partial y^*}A_{\mathrm{ML}}$, where $\overline{\partial\rho/\partial y^*}$ is the average horizontal density gradient over the vertical section whose area is $A_{\mathrm{ML}}$. Here $K_H$ is the average horizontal diffusivity over $A_{\mathrm{ML}}$. It is obvious that the horizontal fluxes are also diapycnal in the mixed layer; here we term them and the related eddy diffusivity as ''horizontal'' to distinguish them from those through the lateral portion of the isopycnal (termed as diapycnal). The eddy flux through the lateral section can be parameterized as Eq. (2.7) via the diapycnal diffusivity $K_\rho$. With the datasets used in this work, we will show that with a horizontal diffusivity value cited in the literature [$O(10^7\ \mathrm{cm^2\ s^{-1}})$], the horizontal eddy fluxes through the mixed layer sections are just too small to balance the air–sea fluxes. Their values are at least an order smaller than the vertical eddy fluxes through the bottom of the water volume with a diapycnal diffusivity of 0.1 $\mathrm{cm^2\ s^{-1}}$. Therefore the effect of the horizontal diffusivity can be neglected compared to the vertical one.

Before carrying out the numerical calculations, we need to clarify the meaning of the diffusivity defined above. First, the diffusivity parameterizes the effect of eddy activities, and as such it depends on the timescales of the eddies (perturbations). For the hydrographic climatology used here, the mean state is defined as the annual mean, and the eddy fluctuations are defined as deviations from the annual mean. For areas with large seasonal variations (e.g., the northern Indian Ocean), the fluctuations are by no means small. Second, all the equations [(2.1)–(2.7)] were formulated for the annual mean state of the quantities; the statements are valid as far as the parameters/quantities are taken as their annual mean values. In the equations the isopycnal surface $A_\rho$ is taken as its annual mean position (remember that the quantities without primes are the annual means), and the eddy diffusivity defined in (2.7) is the averaged value over this annual mean surface and parameterizes the eddy fluxes with respect to the annual means. The instantaneous isopycnal may migrate back and forth around its annual mean position. For the monsoon-dominated northern Indian Ocean, it can be shown from Levitus et al. (1994) that the isopycnal 22.0 $\sigma_\theta$ shifts around its annual mean position at the sea surface (Fig. 4b), enclosing the smallest area in fall (roughly southward from Sri Lanka along 80°E to about 8°S and then eastward) and enclosing the biggest area in spring and summer (roughly southward from west India along about 65°E to about 13°S and then eastward). The isopycnal migrations are smaller in the Bay of Bengal, as the air–sea heat flux and freshwater input are out of phase due to the delay of runoff. The conservation equation following an instantaneous (time dependent) isopycnal is outlined in the following paragraph, where the parameters are time dependent (instead of the annual means as in all other paragraphs).

For simplicity, ignoring the runoff, the throughflow, and the molecular diffusion, the instantaneous density equation is

$$\frac{\partial\rho}{\partial t} + \nabla\cdot(\mathbf{V}\rho) = Q_\rho. \tag{2.8}$$

Taking the ensemble mean in time of (2.8) results in Eq. (2.1). Instead, if we follow the migrating isopycnal $A_\rho(t)$, integration of Eq. (2.8) over a water volume bounded by $A_\rho(t)$ and the air–sea interface $A_s(t)$ (as well as the coastline $A_c$ where applicable) (Fig. 1a) yields

$$\int_{v(t)} \frac{\partial\rho}{\partial t}\, dv + \int_{A_\rho(t)} V_n(t)\rho(t)\, dA = \int_{A_s(t)} Q_\rho(t)\, dA, \tag{2.9}$$

where $v(t)$ is the water volume. Along the isopycnal, $\rho(t)$ is constant, and from the continuity equation at time $t$, the second term on the left-hand side vanishes, and Eq. (2.9) becomes

$$\int_{v(t)} \frac{\partial\rho}{\partial t}\, dv = \int_{A_s(t)} Q_\rho(t)\, dA. \tag{2.10}$$

Equation (2.10) states that, if one follows a moving isopycnal, the integral of the density changing rate over the water volume is determined by the rate of density input over the sea surface. This temporal change rate in turn determines the moving rate of the isopycnal in space. Equation (2.10) is simple, but its application is more complicated than for the annual mean and is being dealt with separately. In the following, we first describe the annual mean air–sea fluxes and water-mass formation rates, followed by the computation of the average diapycnal diffusivities for the annual mean isopycnals.

## 3. Air–sea interaction and water mass formation in the Indian Ocean

The air–sea heat and freshwater fluxes are taken from the atlas of da Silva et al. (1994). (These data can be viewed at the World Wide Web site http://ingrid.ldgo.columbia.edu.) This atlas is based on the raw observational COADS data (Slutz et al. 1985), but more advanced techniques and better quality control were used than in Slutz et al. and Oberhuber (1988). Corrections were made on the biased wind speed, cloudiness, and present weather (PW). (However, biases in sea surface temperature, air temperature, and dewpoint temperature were not corrected.) Air–sea heat and freshwater fluxes were computed through bulk formulas, in which the drag coefficients were stability dependent. A linear inverse technique was also used to adjust the coefficients to satisfy the global conservation of heat and freshwater. (This adjustment corrected an imbalance that averaged to 30.2 $\mathrm{W\ m^{-2}}$ globally.) Precipitation data are also available from the NASA MSU (Microwave Sounding Units) measurements (Spencer et al. 1994) and are

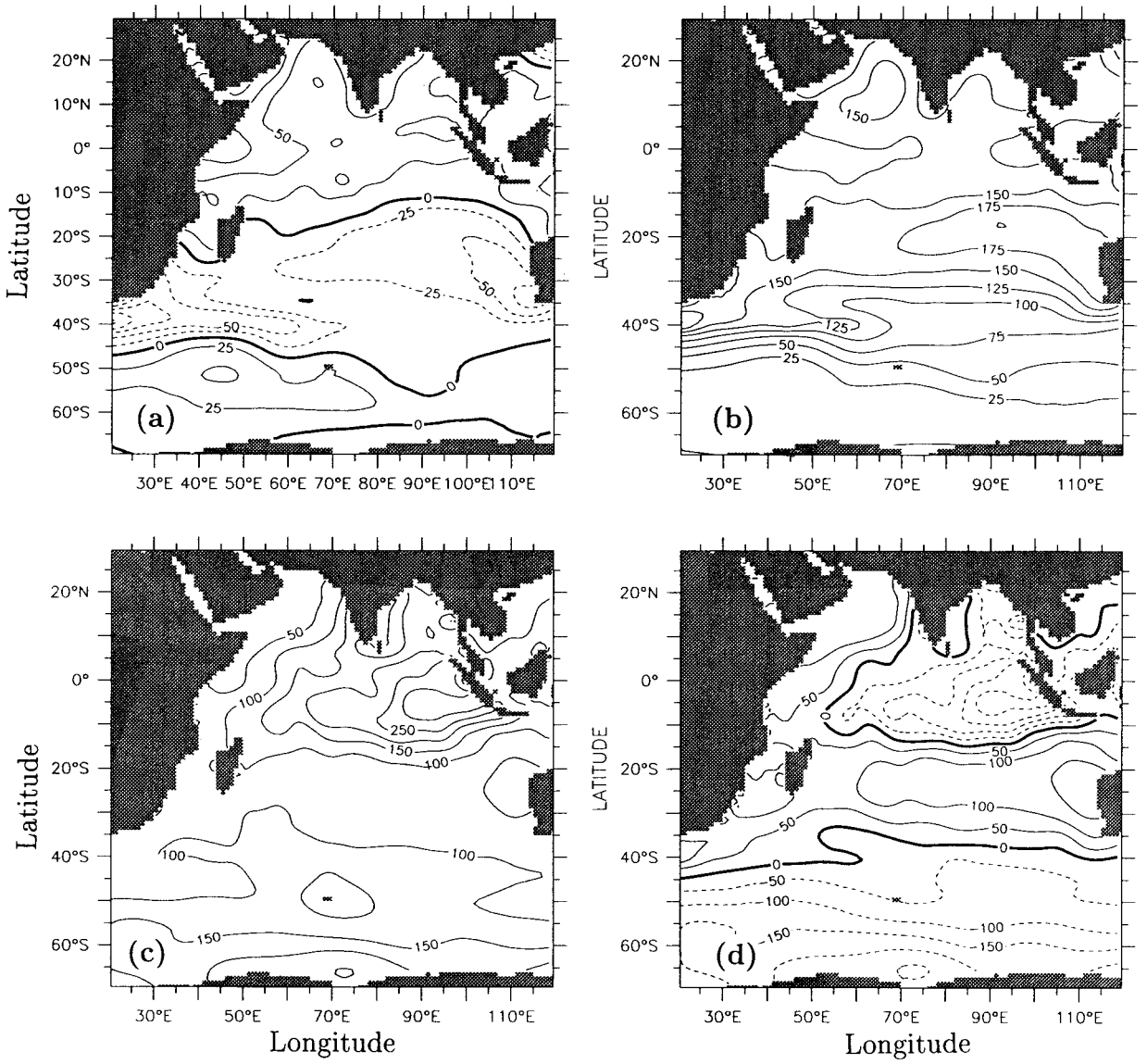


FIG. 2. Air–sea fluxes over the Indian Ocean from da Silva et al. (1994): (a) net heat into the ocean (W m$^{-2}$); (b) evaporation rate (cm yr$^{-1}$); (c) precipitation rate (cm yr$^{-1}$); and (d) $E - P$ flux (cm yr$^{-1}$).

consistent with da Silva et al. The data resolution is 1° × 1° in space and monthly in time with time coverage from 1945 to 1989.

The density flux into the ocean from the atmosphere is computed as

$$Q_\rho = \rho_s(\alpha F_T + \beta F_S) \tag{3.1}$$

and the buoyancy flux into the ocean as $B = -gQ_\rho$, where $\alpha$ and $\beta$ are the thermal expansion and saline contraction coefficients and $\rho_s$ is the density at sea surface. Here $F_T = -Q_{\text{net}}/\rho_s c_p$ and $F_S = (E - P)S/(1 - S/1000)$, in which $Q_{\text{net}}$ is the net heat flux into the ocean, and $S$ the surface salinity, taken from the Levitus et al. (1994) annual mean climatology.

### *a. Surface heat flux*

The climatological annual-mean net sea surface heat flux into the ocean is shown in Fig. 2a for the Indian Ocean and the corresponding Southern Ocean sector. At the largest scale, the ocean receives heat from the atmosphere north of about 20°S, loses heat in the subtropical region between about 20°S and 45°S, and gains a small amount of heat in the circumpolar region. The most intense heat loss occurs in the Agulhas retroflection, with an intensity of about −100 W m$^{-2}$, analogous to the large heat loss regions associated with the Gulf Stream and Kuroshio. The most intensive heat gain in the Indian Ocean occurs along the Arabian coast region

(about 80 W $m^{-2}$), decreasing southeastward. This pattern corresponds well with the shortwave radiation in this area (da Silva et al. 1994), which is a dominant component in the heat budget. The localized minimum net heat gain in the central Arabian Sea is caused by intense evaporation and latent heat loss (Fig. 2b).

Da Silva et al. (1994) do not provide error information for the shortwave radiation flux, thus preventing us from computing errors for the net heat. Instead, we present the seasonal standard deviations for some of the heat components from their atlas. The latent heat flux, the other dominant term in the heat budget, has standard deviations varying from 60 to 80 W $m^{-2}$ north of 40°S, which are about 40 W $m^{-2}$ smaller than the annual mean values of the latent heat flux (100–120 W $m^{-2}$). In the circumpolar region, however, both the latent heat flux and its standard deviation are small and of the same magnitude, varying between zero (near Antarctica) and 60 W $m^{-2}$ (near 45°S). The longwave radiation flux, varying between 40 and 65 W $m^{-2}$ in the Indian Ocean and the circumpolar region, has standard deviations of 15 W $m^{-2}$ or smaller. On the other hand, the small sensible heat flux (of 5–10 W $m^{-2}$) has standard deviations of the same or even larger magnitude (of 10–30 W $m^{-2}$). Generally, the annual-mean net heat flux has larger seasonal standard deviations at high latitudes.

### b. Evaporation and precipitation

The maximum annual-mean evaporation rate in the Indian Ocean is about 175 cm $yr^{-1}$ along about 20°S and generally decreases southward and northward except for localized maxima in the central Arabian Sea and south of Africa (Fig. 2b). The evaporation rate is about 130 cm $yr^{-1}$ in the northern Indian Ocean north of 10°S and is small (about 25 cm $yr^{-1}$) in the circumpolar/Southern Ocean region. The seasonal standard deviation for the annual mean evaporation has a similar spatial structure but with a smaller magnitude north of about 40°S. Farther south they are about the same.

Precipitation in the Indian Ocean (Fig. 2c) has the opposite spatial structure to that of the evaporation: its minimum (about 75 cm $yr^{-1}$) is in the subtropical zone along 25°S. The maximum (of about 300 cm $yr^{-1}$) is located in the eastern equatorial Indian Ocean. Precipitation in the Arabian Sea and along the west coast is low (below 50 cm $yr^{-1}$). In contrast, precipitation is high in the Bay of Bengal, especially along the east coast (above 180 cm $yr^{-1}$). The precipitation has relatively large seasonal variations: the seasonal standard deviations are generally larger than the precipitation rates, although their spatial patterns are similar. In addition to the traditional estimation from ship observations, the NASA MSU started monitoring precipitation in 1979 between 60°S and 60°N. The differences between the NASA annual-mean precipitation rate in the Indian Ocean from 1979 to 1994 and that of da Silva et al. (1994) are small and less than 35 cm $yr^{-1}$ north of 40°S, but are larger farther south.

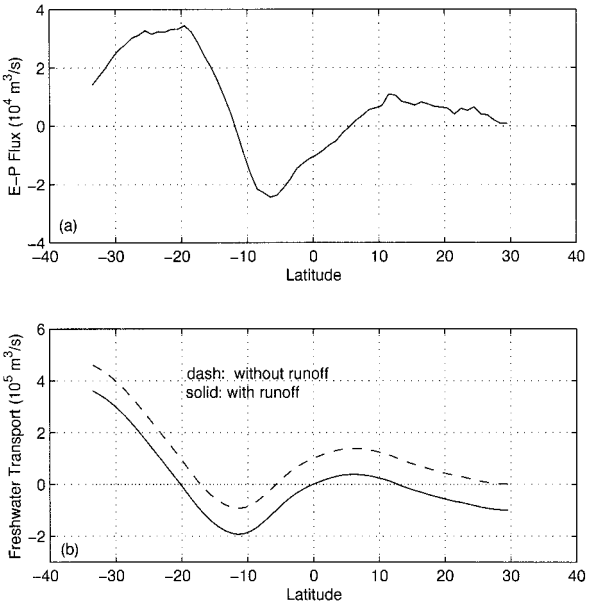


FIG. 3. (a) Zonally integrated $E - P$ flux in the Indian Ocean; (b) freshwater transports integrated from the northern Indian coast: dashed line does not include river runoff.

The annual mean evaporation minus precipitation ($E - P$) is shown in Fig. 2d. In the subtropical region centered along 25°S, evaporation exceeds precipitation and the ocean loses freshwater at a rate of about 100 cm $yr^{-1}$. A freshwater loss at about the same rate also happens in the Arabian Sea, especially in the northwest. On the other hand, the northeast Indian Ocean east of about 70°E and north of about 10°S gains freshwater at the surface, with a maximum rate of about 150 cm $yr^{-1}$ near 5°S, 90°E. South of about 40°S, the ocean also gains freshwater, and in the circumpolar region the rate reaches 100–200 cm $yr^{-1}$ with larger seasonal standard deviations.

The zonally integrated $E - P$ flux for the Indian Ocean (Fig. 3a) shows a loss of freshwater north of about 5°N. Between 5°N and 12°S, the ocean gains freshwater, with a maximum rate of $2.5 \times 10^4$ $m^3$ $s^{-1}$ at 6°S. South of 12°S, the ocean loses freshwater again, with a maximum rate of $3.5 \times 10^4$ $m^3$ $s^{-1}$ at about 20°S. Integrated from the northern coast, the freshwater transport in the Indian Ocean caused by the air–sea interaction is shown in Fig. 3b (dashed line) as a function of latitude. This is similar to that of Wijffels et al. (1992) based on Baumgartner and Reichel (1975). On the other hand, the solid line, obtained by adding the river runoff from the northern coast (cf. section 4b for sources), shows that the runoff is important in determining the direction of freshwater transport in the Indian Ocean. North of about 12°N, there are southward freshwater transports, with a maximum of about $0.1 \times 10^6$ $m^3$ $s^{-1}$ at the northern coast (from runoff). Freshwater is trans-

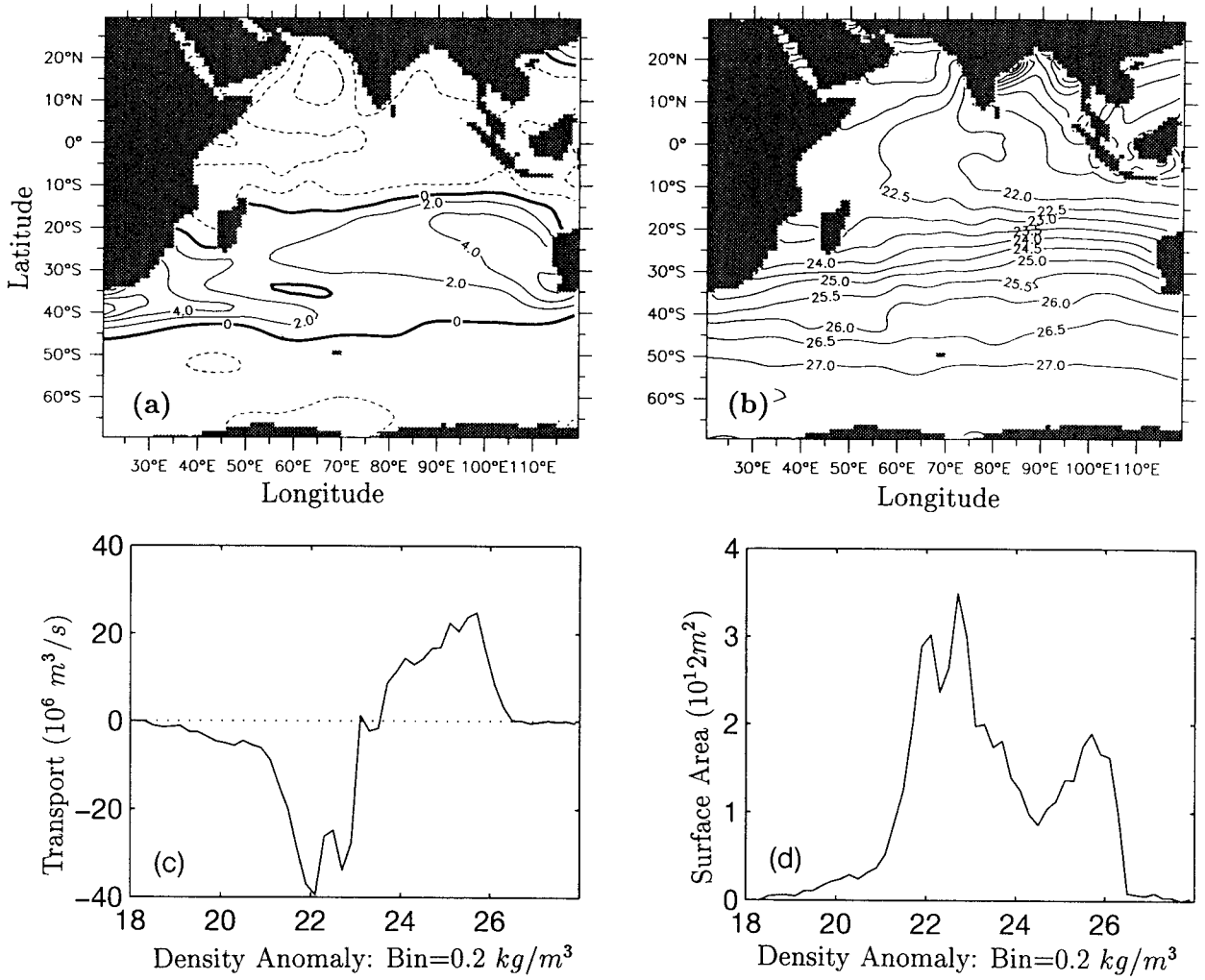


FIG. 4. (a) Air–sea surface density flux ($10^{-6}$ kg m$^{-2}$ s$^{-1}$) into the ocean [based on da Silva et al. (1994)]; (b) sea surface potential density anomaly (Levitus et al. 1994); (c) water mass formation rates in surface density classes with a bin of 0.2 kg m$^{-3}$; (d) sea surface area ($10^{12}$ m$^2$) of each density class.

ported northward (weakly) between 12°N and the equator. Between the equator and 20°S, freshwater is transported southward again with a maximum rate of about $0.2 \times 10^6$ m$^3$ s$^{-1}$ at 12°S. There are net northward freshwater transports again south of 20°S, with rates increasing southward to 35°S where the Indian Ocean opens to the other oceans.

### c. *Surface density/buoyancy flux and water mass formation rates*

The annual-mean net density flux into the ocean is shown in Fig. 4a. The Indian Ocean loses density (gains buoyancy) north of about 12°S, with rates of $-2$ to $-4$ ($\times 10^{-6}$ kg m$^{-2}$ s$^{-1}$). The density loss is caused by gains in both heat and freshwater in this area except in the subdomain of the Arabian Sea, where the effect of heat gain exceeds the effect of freshwater loss. In the subtropics between 12°S and 45°S, the Indian Ocean gains density at rates of 2 to 5 ($\times$ $10^{-6}$ kg m$^{-2}$ s$^{-1}$), due to losses in both heat and freshwater. Farther south, there are weak density losses by the ocean, due to both the net heat and freshwater gains. The most intensive density gain occurs west of Australia and just south of Africa.

Speer and Tziperman (1992) and Speer et al. (1995) computed the water-mass formation rates in density classes for the North Atlantic and the global ocean. Following their method, the density flux of Fig. 4a is integrated over the surface density strips with a bin of 0.2 kg m$^{-3}$ (Fig. 4b) and divided by the bin width (0.2 kg m$^{-3}$) to derive the water-mass formation rates ($dQ_\rho/d\rho$), as shown in Fig. 4c together with the surface area for the surface density classes (Fig. 4d). Figure 4c shows that air–sea interaction lightens the light water masses of density less than 23.0 $\sigma_\theta$ and increases the density of the denser water, since

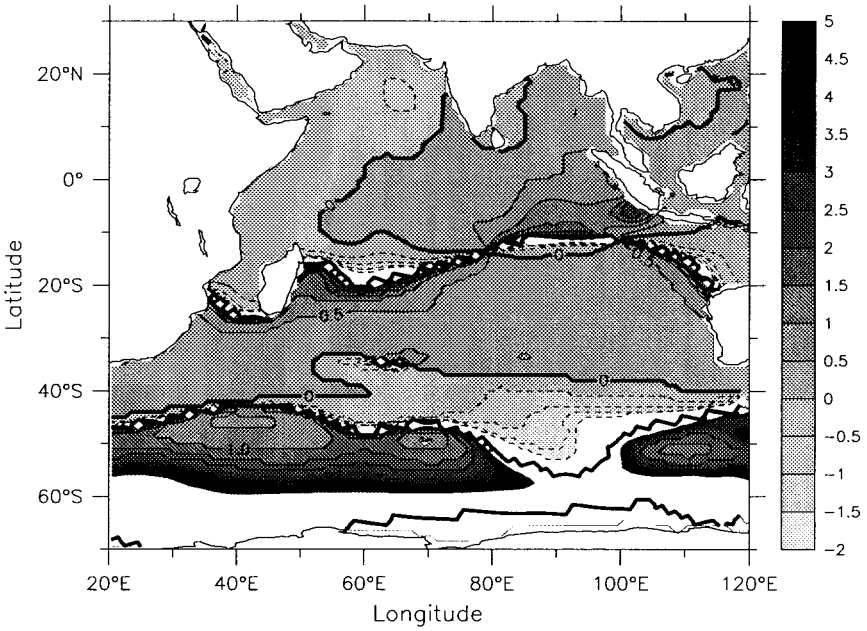


FIG. 5. Ratio of air–sea freshwater flux over heat flux toward the density flux in the Indian Ocean.

the surface isopycnal 23.0 $\sigma_\theta$ lies near the zero line of the sea surface density flux (Figs. 4a,b). Although the density flux is relatively uniform over the area north of the zero line (Fig. 4a), a negative peak mass formation rate (into lighter water) appears near surface density 22.0 $\sigma_\theta$, which spans a larger area than other density classes (Fig. 4b). A positive peak in the water mass formation (into denser water) appears near 26.0 $\sigma_\theta$ (Fig. 4c), corresponding to the area of intensive density gain between Australia and the tip of South Africa (Fig. 4a). The shape of the formation rate in Fig. 4c is similar to the results of Speer et al. (1995), but the peak of the negative formation rate is greater in the present calculation: $-4.0 \times 10^7$ m$^3$ s$^{-1}$ versus $-2.0 \times 10^7$ m$^3$ s$^{-1}$. The peak location shifts from 21.5 to 22.1 $\sigma_\theta$. The positive peak formation rate is about the same as in Speer et al. (1995), but the location shifts from about 24.5 to 25.7 $\sigma_\theta$. The differences of this work from Speer et al. (1995) show the differences of the marine surface data used in the two works. It is believed that the dataset used in this work took into account more corrections and bias of the raw observational data (da Silva et al. 1994).

Although both air–sea heat and freshwater fluxes contribute to the density flux, comparisons among Figs. 4a (the density flux), 2d (the $E - P$ flux), and 2a (the net heat flux) show that the density flux structure more closely follows that of the heat flux, suggesting the dominance of the thermal process over the freshwater exchange process in modifying the water mass density. Indeed, the density flux computed from air–sea heat flux only (by setting $E - P = 0$) is very similar to Fig. 4a. The density flux ratio, that is, the ratio of the density flux caused by freshwater over that caused by heat flux, is about 0.2–0.4 in most of the Indian Ocean (Fig. 5) and is only larger than 1.0 near the zero lines of the net heat flux (along 23.0 $\sigma_\theta$ and near 20°S) and in the circumpolar region. The freshwater flux reinforces the heat flux toward changing the density in most areas except in the northwest and in a narrow band around 45°S where they are opposed.

## 4. Diapycnal diffusivity for the Indian Ocean

Using the method outlined in section 2, diapycnal diffusivities were computed for several shallow, closed isopycnals in the Indian Ocean, using the density flux discussed in the previous section and the climatological hydrographic dataset of Levitus et al. (1994). The sea surface isopycnals (Fig. 4b) closely follow surface isotherms (Fig. 8) in most of the Indian Ocean except in the Bay of Bengal where isopycnals are closer to isohalines than to isotherms. As a consequence of the large input of freshwater from precipitation and river runoff, the intensified salinity structure dominates the density distributions in this region. The Bay of Bengal has the lightest water in the Indian Ocean; isopycnals outcrop from the coastal area southwestward and then southward (Fig. 4b). The computation of diapycnal diffusivities follows the same direction: starting from the Bay of Bengal for the surface water and moving deeper and south(west)ward to about 35°S, with density anomaly ranges from 20.2 to 25.0. The densest isopycnal considered here has a maximum depth of about 150 m; thus the term ''isopycnal/diapycnal'' in this section can refer either to density or potential density without a practical difference in the results. The average diapycnal diffu-

TABLE 1. Diapycnal diffusivity in the Indian Ocean. The values of $K$ outside the parentheses are from air–sea buoyancy flux only, while those in the parentheses include the effect of the Indonesian Throughflow and river runoff.

| $\sigma_\theta$ | Principal location | Approximate depth (m) | Density flux ($10^7$ kg s$^{-1}$) | Surface area ($10^{13}$ m$^2$) | $-d\rho/dz$ ($10^{-2}$ kg m$^{-4}$) | $K_\rho$ (cm$^2$ s$^{-1}$) |
|---|---|---|---|---|---|---|
| 20.2 | Bay of Bengal | 20 | −0.47 | 0.11 | 5.0 | 0.9 (1.2) |
| 21.0 | Bay of Bengal | 30 | −0.91 | 0.23 | 3.6 | 1.1 (1.3) |
| 21.5 | NE Indian Ocean | 40 | −1.51 | 0.42 | 3.0 | 1.2 (1.3) |
| 22.0 | NE Indian Ocean | 60 | −3.14 | 1.00 | 2.6 | 1.2 (1.3) |
| 23.0 | North of 20°S excl. Arabian Sea | 75 | −6.14 | 2.44 | 3.0 | 0.8 (0.9) |
| 25.0 | North of 35°S | 120 | −4.27 | 3.86 | 2.7 | 0.4 (0.5) |

sivities for six isopycnals in the Indian Ocean are summarized in Table 1 and Fig. 1a. Their locations and depth ranges are shown in Fig. 6. The values in the parentheses in Table 1 and Fig. 1a include the the Indonesian Throughflow and river runoff as discussed in sections 4a and 4b.

Generally the diapycnal diffusivity is relatively constant in the northeast and decreases poleward after the isopycnal passes the equator and deepens. The lightest isopycnal in Fig. 6, 21.0 $\sigma_\theta$, encloses the freshest and lightest water in the Bay of Bengal. It more or less follows the coastline (Fig. 6a), and Fig. 4a shows an intensive density loss there. The isopycnal deepens from its outcrop line at about 10°N to about 30 m at the coast. Integrating the air–sea density flux over an area bounded by the coast and this isopycnal yields a density loss of $-9.1 \times 10^6$ kg s$^{-1}$ over an area of $2.3 \times 10^{12}$ m$^2$. The average eddy density flux across this isopycnal is thus $-3.95 \times 10^{-6}$ kg m$^{-2}$ s$^{-1}$. From the Levitus et al. (1994) hydrographic data, the mean diapycnal density gradient averaged over this isopycnal surface is $-3.6 \times 10^{-2}$ kg m$^{-4}$. Thus the average diapycnal eddy diffusivity is 1.1 cm$^2$ s$^{-1}$ if only air–sea flux is used. (It increases to 1.3 cm$^2$ s$^{-1}$ when the Indonesian Throughflow and river runoff are included.)

The isopycnal 22.0 $\sigma_\theta$ encloses the northeast Indian Ocean north of about 10°S east of 80°E (Fig. 6b). It extends to about 50-m depth in the northeast. The total density loss over the sea surface area of $1.0 \times 10^{13}$ m$^2$ is $-3.14 \times 10^7$ kg s$^{-1}$, which gives a mean eddy flux of $3.15 \times 10^{-6}$ kg m$^{-2}$ s$^{-1}$ across this isopycnal. The diapycnal density gradient has a mean value of $-2.6 \times 10^{-2}$ kg m$^{-4}$, and this gives a mean diapycnal diffusivity of 1.21 cm$^2$ s$^{-1}$. Farther south, the isopycnal 23.0 $\sigma_\theta$ encloses the whole upper Indian Ocean north of about 20°S excluding the Arabian Sea. It reaches 70-m depth in the Bay of Bengal (Fig. 6c). The total air–sea density flux over its area of $2.44 \times 10^{13}$ m$^2$ is $-6.14 \times 10^7$ kg s$^{-1}$, resulting in a mean eddy flux of $2.52 \times 10^{-6}$ kg m$^{-2}$ s$^{-1}$ across the isopycnal. The mean diapycnal density gradient on this isopycnal is $-0.03$ kg m$^{-4}$, and this gives a mean diapycnal diffusivity of 0.84 cm$^2$ s$^{-1}$.

The isopycnal 25.0 $\sigma_\theta$ encloses the whole upper Indian Ocean north of about 35°S. This isopycnal deepens from the sea surface at about 35°S northward to about 120 m depth along 15°S and then shoals to about 100 m farther north (Fig. 6d). The isopycnal also locally shoals up to about 80-m depth near 7°S, 60°E and to about the same depth (80 m) near the Arabian coast. The total air–sea density loss over this area (of $3.86 \times 10^{13}$ m$^2$) is $-4.27 \times 10^7$ kg s$^{-1}$, which is lower than at $\sigma_\theta = 23.0$, due to the density gain around 20°S (cooling and excessive $E - P$). This gives a smaller mean diapycnal eddy density flux of $1.1 \times 10^{-6}$ kg m$^{-2}$ s$^{-1}$. Combined with a mean diapycnal density gradient of $-2.7 \times 10^{-2}$ kg m$^{-4}$, an average diapycnal diffusivity of 0.4 cm$^2$ s$^{-1}$ is obtained.

### *a. Effect of the Indonesian Throughflow*

As mentioned in section 2, in the presence of the Indonesian Throughflow and river runoff, the divergence of the advective flux for density by the annual mean circulation generally does not vanish, as the inflow from the Indonesian passage/river runoff is less dense than the outflow across the isopycnals in the south. (The continuity equation requires the net volume transport out of the isopycnal surface to be equal to that from the Indonesian Throughflow/river runoff annually to maintain the annual mean sea level.) Assume that the volume transport through the passage and above the isopycnal (e.g., 23.0 $\sigma_\theta$) is $V_i$, and the associated density flux (integral of $\mathbf{V}\rho$) is $M_i$. For a steady state, the volume transport out of the isopycnal surfaces should also be $V_i$, and this results in a density flux of $M_o = V_i \times \rho_o$, where $\rho_o$ is the density at the isopycnal concerned. As a consequence, the net density flux divergence caused by the throughflow is $M_i - M_o$, which should be added to the buoyancy budget between the air–sea flux and the diapycnal flux.

The Indonesian Throughflow varies seasonally, and even the annual mean transport cited in the literature varies (Lukas et al. 1996). The XBT data obtained by Meyers et al. (1995) and used by Morris (1996) has a time coverage of over 10 years (1983–1994) and thus is closer to a climatological mean than other datasets available. Using this dataset and a reference level of zero velocity at 740 m, a geostrophic volume transport of $-2.28$ Sv and a density anomaly transport of $-5.1 \times 10^7$ kg s$^{-1}$ above 23.0 $\sigma_\theta$ are obtained, using the program provided by Morris (1996). Using the FSU pseudo wind data for that time period (Stricherz et al.

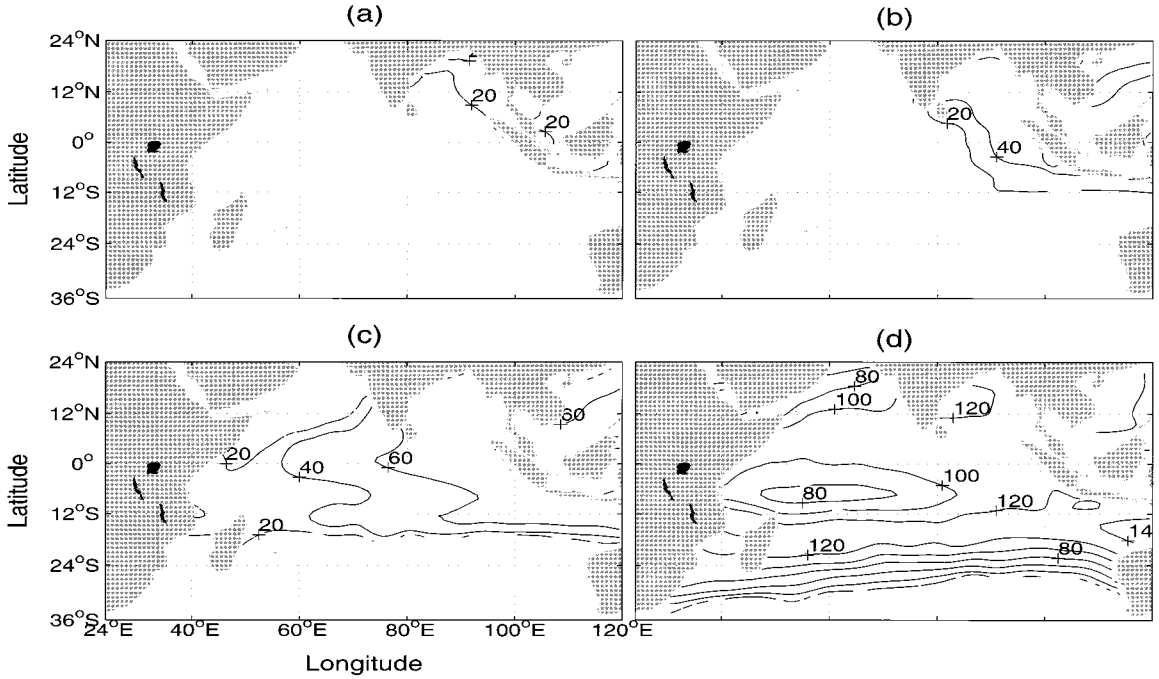


FIG. 6. Geographical locations and depths of the isopycnals in the Indian Ocean: (a) $\sigma_\theta = 21.0$, (b) $\sigma_\theta = 22.0$, (c) $\sigma_\theta = 23.0$, and (d) $\sigma_\theta = 25.0$. Contour intervals are 20 m.

1992), an Ekman volume transport of $-2.34$ Sv and a density anomaly transport of $-5.15 \times 10^7$ kg s$^{-1}$ above 23.0 $\sigma_\theta$ are obtained. Adding the above two components results in the total volume and density anomaly transports through the Indonesian passage and above 23.0 $\sigma_\theta$ as $V_i = -4.62$ Sv and $M_i = -1.03 \times 10^8$ kg s$^{-1}$ respectively. The net density flux divergence by the throughflow is thus $M_{\text{net}} = M_i - M_o = -0.38 \times 10^7$ kg s$^{-1}$, which is only about 6% of the air–sea density flux ($-6.14 \times 10^7$ kg s$^{-1}$) for this isopycnal (23.0 $\sigma_\theta$). Including the throughflow increases the mean diapycnal diffusivity from 0.84 to 0.89 cm$^2$ s$^{-1}$ for 23.0 $\sigma_\theta$.

However, farther south, for the water volume bounded by isopycnal 25.0 $\sigma_\theta$ (north of about 35°S), the net surface buoyancy gain decreases as buoyancy loss appears in midlatitudes. At the same time, the volume and freshwater transports through the Indonesian passage above 25.0 $\sigma_\theta$ increase (over those above 23.0 $\sigma_\theta$) and thus increase the impact of the Indonesian Throughflow on the buoyancy budget. Using the procedures and datasets described above, the divergence of the density flux caused by the throughflow is $M_{\text{net}} = -1.45 \times 10^7$ kg s$^{-1}$ for isopycnal 25.0 $\sigma_\theta$. This is about 34% of the air–sea density flux ($-4.27 \times 10^7$ kg s$^{-1}$) for the same isopycnal, and the diapycnal diffusivity increases from 0.40 to 0.54 cm$^2$ s$^{-1}$ when the throughflow is included.

### b. Effect of river runoff

River runoff from the Ganges, Brahmaputra, Irrawaddy, and Godavari Rivers clearly affects the stratification in the Bay of Bengal (Fig. 4b). Another major river with a lower discharge rate is the Indus, which flows into the Arabian Sea. The main sources for the river runoff data are 1) Baumgartner and Reichel (1975), 2) UNESCO's (1978) World Water Balance and Water Resources of the Earth, and 3) UNESCO's table series of Discharge of Selected Rivers of the World (Vol. 1, 1969; Vol. 2, 1971; Vol. 3, parts 1–5, 1969–1992). (The Global Runoff Data Center in Germany under the auspices of the WMO maintains some of the data.) Data from source 3 show that the annual mean runoff from the Ganges fluctuates around a mean value of $1.2 \times 10^4$ m$^3$ s$^{-1}$ and that from Brahmaputra fluctuates around $2.0 \times 10^4$ m$^3$ s$^{-1}$ (Fig. 7). Data from source 2 show that the Ganges–Brahmaputra system has an annual mean flux rate of $3.9 \times 10^4$ m$^3$ s$^{-1}$ and the flow from the Irrawaddy has an annual mean rate of $1.5 \times 10^4$ m$^3$ s$^{-1}$. This dataset also gives a total flow rate of $11.6 \times 10^4$ m$^3$ s$^{-1}$ into the Indian Ocean from Asia. Source 1 gives a runoff rate of $10 \times 10^4$ m$^3$ s$^{-1}$ into the north Indian Ocean. Considering the uncertainty of the runoff, we chose a rate of $8 \times 10^4$ m$^3$ s$^{-1}$ into the Bay of Bengal and a rate of $10 \times 10^4$ m$^3$ s$^{-1}$ into the whole Indian Ocean basin.

For the upper coastal water bounded by 20.2 $\sigma_\theta$ in the Bay of Bengal, if the runoff rate of $8 \times 10^4$ m$^3$ s$^{-1}$ is converted into a pseudo net precipitation rate over the sea surface area bounded by this isopycnal and the coast ($1.07 \times 10^{12}$ m$^2$), it amounts to $7.5 \times 10^{-8}$ m s$^{-1}$ or 236.0 cm yr$^{-1}$. This number is larger than the actual annual mean $P - E$ in this area (about 50 cm yr$^{-1}$; Fig.

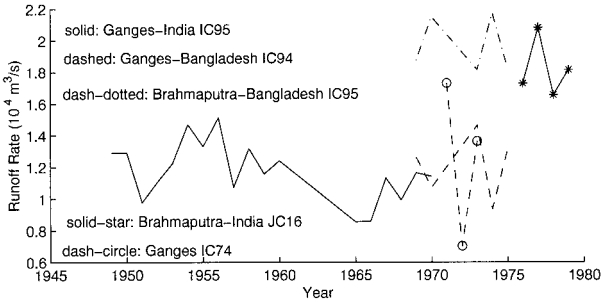


FIG. 7. Time series of discharge rates into the northern Indian Ocean from UNESCO (1969–1992).

2d). For the steady state, this inflow of water from the rivers must cross the 20.2 $\sigma_\theta$ isopycnal to maintain the climatological annual mean sea level. This causes a net density loss at a rate of $-8 \times 10^4 \times (1020.2 - 1000.0)$ kg $s^{-1} = -1.62 \times 10^6$ kg $s^{-1}$ for the water volume bounded by this isopycnal and the coast. Compared to the surface density flux of $-4.68 \times 10^6$ kg $s^{-1}$, the runoff contributes about 35% in the buoyancy/density budget for this water volume, although the runoff rate is larger than the surface $E - P$ rate. This is because heating dominates freshening in changing the surface buoyancy (Fig. 5). By including the river runoff in the buoyancy budget for this water volume, the diapycnal eddy diffusivity over this isopycnal increases from 0.9 to 1.2 $cm^2$ $s^{-1}$.

For the water volume bounded by isopycnal 21.0 $\sigma_\theta$ and the coast, the density flux loss caused by the river runoff is $-8.0 \times 10^4 \times (1021.0 - 1000.0)$ kg $s^{-1} = -1.68 \times 10^6$ kg $s^{-1}$, or about 16% of the surface density flux ($9.06 \times 10^6$ kg $s^{-1}$). Including the runoff increases the diapycnal diffusivity for this isopycnal from 1.1 to 1.3 $cm^2$ $s^{-1}$. Moving farther south and for larger water volume, the effect of runoff decreases in the buoyancy budget. Compared to the surface fluxes, the buoyancy gain caused by runoff amounts to 10%, 6%, 3%, and 6% for the water volume bounded by the coast and the isopycnals $\sigma_\theta = 21.5$, 22.0, 23.0, and 25.0, respectively. The diapycnal eddy diffusivity increases from 1.2, 1.2, 0.8, 0.4 to 1.3, 1.3, 0.9, and 0.42 $cm^2$ $s^{-1}$ for those isopycnals respectively (Table 1 and Fig. 1a).

### *c. Discussion*

In the above sections we computed the mean diapycnal diffusivity values for various isopycnals in the Indian Ocean. Although variations of the diapycnal diffusivity along the isopycnals cannot be accessed from this kind of calculation, we can illustrate the variation of the average diffusivity from one isopycnal to another, and thus its rough variation with space. Figure 1a schematically displays the locations of the isopycnals on which the mean diffusivity values were calculated for the Indian Ocean. The diapycnal diffusivity values are also displayed on this diagram: the numbers in the parentheses include all the buoyancy sources (air–sea fluxes, runoff, and Indonesian Throughflow), while those outside the parentheses include air–sea surface fluxes only.

Similar diapycnal mixing rates (around 1.3 $cm^2$ $s^{-1}$) are found on isopycnals $\sigma_\theta = 20.2$, 21.0, 21.5, and 22.0, whereas farther south (after crossing the equator) and downward the mixing rate decreases (0.9 $cm^2$ $s^{-1}$ on 23.0 $\sigma_\theta$ at depth around 70 m, and 0.5 $cm^2$ $s^{-1}$ on 25.0 $\sigma_\theta$ at depth around 100 m). These values are consistent with the idea that mixing is possibly stronger near the surface and the equator. From 20.2 to 22.0 $\sigma_\theta$, the isopycnals shift southward to include more tropical water, which might increase the mixing. At the same time the isopycnals shift downward, where mixing might decrease. The two effects compensate each other, thus maintaining a quasi-constant average mixing rate. From 22.0 to 25.0 $\sigma_\theta$, the isopycnals encompass more area south of the equator and lie at greater depth; the diapycnal diffusivity decreases monotonically. The results from the following computation of diathermal diffusivity values for isotherms, which straddle the equator, are consistent with the above arguments.

## 5. Diathermal diffusivity in the Indian Ocean

Isotherms are not collocated with isopycnals, so there may be independent information about the geographical distribution of diffusivity if the same calculations are done for potential temperature. The computation here for the diathermal diffusivities mirrors the computation for the diapycnal diffusivities, but we use the heat budget for water volumes bounded by isotherms, the sea surface, and coast. The annual-mean sea surface potential temperature distribution from the Levitus et al. (1994) atlas is shown in Fig. 8. Unlike the surface density, which is the lowest in the Bay of Bengal and increases southwestward, the warmest water straddles the equator. The mean locations and depths for four of the seven isotherms displayed in Fig. 1b are shown in Fig. 9. The average diathermal diffusivities over these isotherms are summarized in Table 2 and schematically displayed in Fig. 1b. The diathermal diffusivity values decrease from the warm center poleward and with depth. In the warmest pool centered around the equator (say, above $\theta = 28.0$°C), the diathermal diffusivity has larger values ($>2.2$ $cm^2$ $s^{-1}$) than the diapycnal diffusivity (of 1.3 $cm^2$ $s^{-1}$) at about the same depth, which also includes the Bay of Bengal water. However, farther south and downward, the isopycnals more and more closely follow the isotherms, and the diathermal and diapycnal diffusivity values converge. The isopycnal 25.0 $\sigma_\theta$ is very close to the isotherm $\theta = 21.0$°C, so the associated diathermal diffusivity calculated from the heat budget is about the same as the diapycnal diffusivity calculated from the buoyancy budget (0.5 $cm^2$ $s^{-1}$).

It is believed that advection and mixing processes occur mainly along isopycnals, and the isopycnal eddy

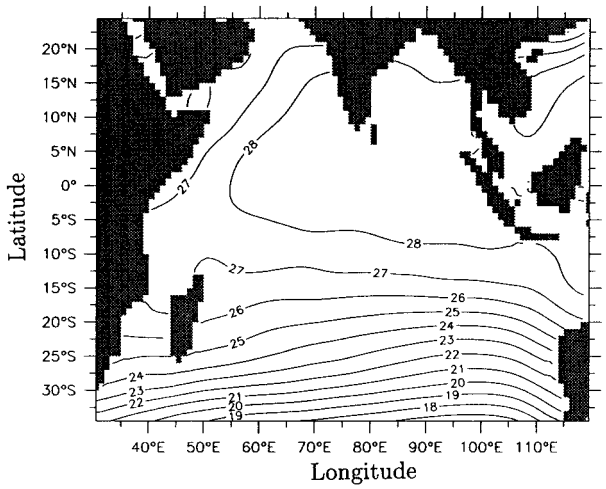


FIG. 8. Annual-mean sea surface potential temperature in the Indian Ocean (from Levitus et al. 1994).

diffusivity is believed to be about $10^6$ times larger than the diapycnal one. If isotherms tilt across isopycnals, the diathermal diffusivity may simply include a component of the much larger isopycnal diffusivity (i.e., the isopycnal diffusivity times the sine of the angle between the isotherm and the isopycnal). This effect is largest in the northeast Indian Ocean because of the large freshwater input there. Unfortunately, the geometric relation between the isotherms and the isopycnals in this region is too complicated to be quantified. McWilliams et al. (1996) also discussed this issue in a numerical model, in which mesoscale fluxes were represented by isopycnally oriented, quasi-adiabatic parameterization. The microscale fluxes occurred with a small vertical diffusivity of $O(0.1)$ cm$^2$ s$^{-1}$ in the predominantly stably stratified warm water sphere, yet they were shown to be sufficient to provide the primary balance against surface forcing. In their case, the isotherms closely aligned with the isopycnals, thus the heat balance for water volumes bounded by isotherms and air–sea surface was primarily between the surface fluxes and the microscale fluxes across the isotherms. Contribution from isopycnal diffusive heat fluxes could be neglected. On the other hand, the isohalines dealigned with the isopycnals, thus the mesoscale isopycnal diffusion fluxes also contributed significantly to the freshwater budgets for water volumes bounded by isohalines.

## 6. Global calculations

The above computations and analyses are easily extended to the global ocean. In the following we present the diapycnal diffusivity distributions based on the sea surface density distribution of Fig. 10 from the atlas of Levitus et al. (1994).

### *a. The Indian–Pacific system*

One of the uncertainties in the calculation for the Indian Ocean is the strength of the Indonesian Through-

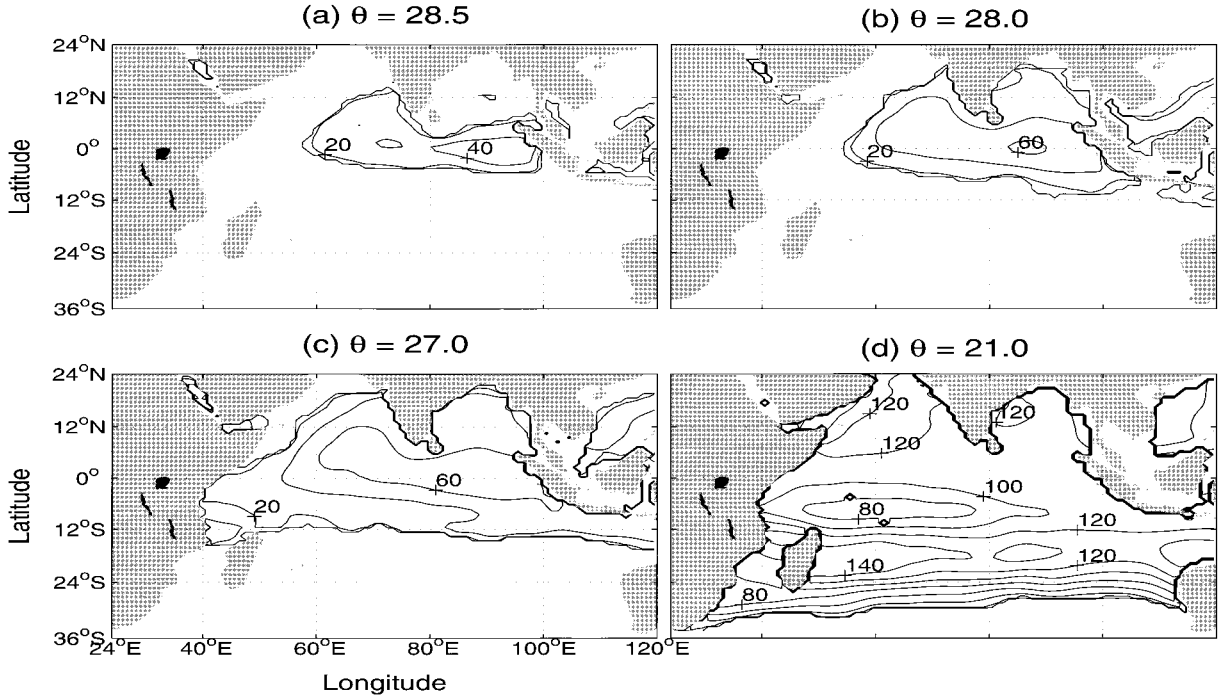


FIG. 9. Geographical locations and depths for four mean isotherms in the Indian Ocean (from Levitus et al. 1994). Contour intervals are 20 m.

TABLE 2. Diathermal diffusivity in the Indian Ocean estimated from heat budget.

| $\theta$ (°C) | Principal location | Approximate depth (m) | Heat flux ($10^{14}$ W) | Surface area ($10^{12}$ m$^2$) | $d\theta/dz$ ($10^{-2}$ K m$^{-1}$) | $K_\theta$ (cm$^2$ s$^{-1}$) |
|---|---|---|---|---|---|---|
| 29.0 | 5°N–1°S | 15 | 0.38 | 0.96 | 0.8 | 12.0 |
| 28.8 | 8°N–5°S | 30 | 1.17 | 3.22 | 2.0 | 4.4 |
| 28.5 | 10°N–5°S | 40 | 2.38 | 6.70 | 2.3 | 4.0 |
| 28.3 | 15°N–7°S | 50 | 3.48 | 9.58 | 2.6 | 3.5 |
| 28.0 | 20°N–10°S | 55 | 4.47 | 12.4 | 3.9 | 2.2 |
| 27.0 | 20°N–15°S | 65 | 8.23 | 22.3 | 7.0 | 1.3 |
| 21.0 | 25°N–30°S | 120 | 6.30 | 38.7 | 8.2 | 0.5 |

flow. Based on the XBT data of Meyers et al. (1995) and the FSU pseudo wind data (Morris 1996), the Indonesian Throughflow contributes about 34% in the buoyancy budget for the water volume bounded by 25.0 $\sigma_\theta$ and the sea surface in the Indian Ocean (section 4a). In this section we treat the Indian and the Pacific Oceans as one system, thus removing the uncertainty caused by the throughflow. The diapycnal diffusivity values for several isopycnals are shown in Table 3. For the water mass in the Bay of Bengal and around the Indonesian seas ($\sigma_\theta$ = 21.5, depth ~40 m), the warm pool water bounded by 22.0 $\sigma_\theta$ (depth ~60 m), and the tropical water bounded 23.0 $\sigma_\theta$ between about 20°N and 20°S (depth ~100 m) (Fig. 10), the diapycnal mixing rates are about the same as the calculations in the Indian Ocean, with values of 1.3, 1.3, and 0.9 cm$^2$ s$^{-1}$, respectively. However, for the water bounded by 25.0 $\sigma_\theta$ between about 40°N and 40°S in the Indian–Pacific system, the diapycnal diffusivity decreases to 0.1 cm$^2$ s$^{-1}$ from 0.5 cm$^2$ s$^{-1}$ for the Indian Ocean water only. The isopycnal (25.0 $\sigma_\theta$) is deeper (depth about 170 m) and covers a larger midlatitude area (to about 40°N) in the Pacific than in the Indian (depth about 120 m and to the northern coast of the Indian Ocean at about 25°N). The larger diffusivity in the Indian Ocean is consistent with the concept that mixing is stronger in the Tropics and near the ocean surface.

There are also closed isopycnals (intercepting the coast) in the eastern tropical Pacific, bounding the least dense water masses there (Fig. 10). The buoyancy budgets for isopycnals 21.5 $\sigma_\theta$ (depth ~25 m) and 22.0 $\sigma_\theta$ (depth ~35 m) yield diapycnal diffusivity values of 1.1 and 0.6 cm$^2$ s$^{-1}$, respectively. These values are smaller than those for isopycnals at similar depths but in the northeast Indian Ocean. (See section 7 for a possible interpretation.)

### b. The Atlantic Ocean

Diapycnal diffusivity values for some isopycnals in the Atlantic Ocean are given in Table 4. As shown in

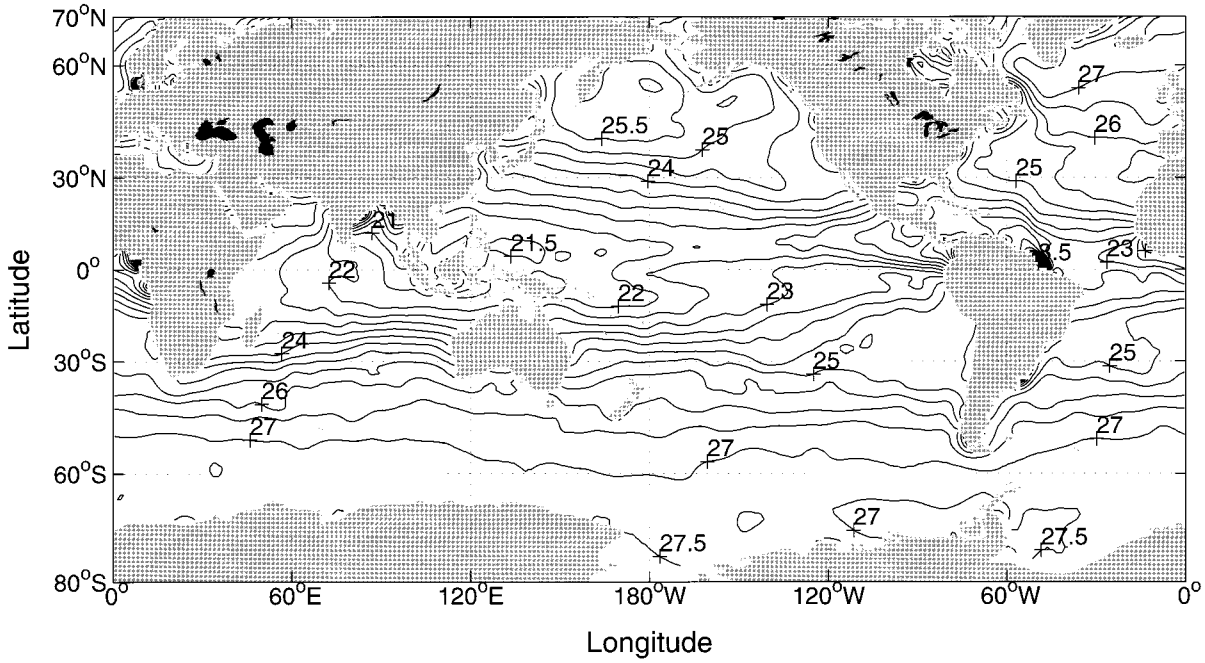


FIG. 10. Annual-mean sea surface potential density anomaly over the global ocean from Levitus et al. (1994), showing the locations in which buoyancy budgets were used to estimate the diapycnal diffusivities. Contour intervals are 0.5 kg m$^{-3}$.

TABLE 3. Diapycnal diffusivity in the Indian–Pacific system. The values of $K$ outside the parentheses are from air–sea buoyancy flux only, while those in the parentheses include the effect of river runofff.

| $\sigma_\theta$ | Principal location | Approximate depth (m) | Density flux ($10^8$ kg s$^{-1}$) | Surface area ($10^{13}$ m$^2$) | $-d\rho/dz$ ($10^{-2}$ kg m$^{-4}$) | $K_\rho$ (cm$^2$ s$^{-1}$) |
|---|---|---|---|---|---|---|
| 21.5 | Bay of Bengal and Indonesian Seas | 40 | −0.32 | 0.90 | 3.0 | 1.2 (1.3) |
| 22.0 | Warm pool | 60 | −0.81 | 3.11 | 2.0 | 1.3 (1.3) |
| 23.0 | 20°N–20°S | 100 | −1.30 | 8.60 | 2.5 | 0.8 (0.9) |
| 25.0 | 40°N–40°S | 170 | −0.49 | 16.4 | 2.3 | 0.1 (0.1) |
| 21.5 | E Tropical Pacific | 25 | −0.09 | 0.29 | 3.2 | 1.1 |
| 22.0 | E Tropical Pacific | 35 | −0.14 | 0.63 | 4.0 | 0.6 |
| 27.5 | Global: 65°N–Antarctic | 400 | −0.59 | 34.4 | 0.8 | 0.2 |

Fig. 10, there are two low-density surface pools in the eastern and western tropical Atlantic, reflecting the runoff from the Amazon and Niger Rivers. The buoyancy budget for the eastern freshwater pool bounded by 23.0 $\sigma_\theta$ (depth ~30 m) yields a diapycnal diffusivity of 0.6 cm$^2$ s$^{-1}$; inclusion of river runoff has little effect. However, the runoff from the Amazon makes a big difference in the buoyancy budget for the western freshwater pool bounded by isopycnal 23.0 $\sigma_\theta$ (depth ~30 m). The diapycnal diffusivity is only 0.05 cm$^2$ s$^{-1}$ without the runoff but increases to 0.4 cm$^2$ s$^{-1}$ with the runoff. These values are smaller than those in the Indian Ocean and the Indian–Pacific system, even though the isopycnals are shallower in the Atlantic than in the other oceans. This may be caused by the stronger stratification in the Atlantic. (See Fig. 11 and discussions in section 7.)

For the tropical waters bounded by 23.5 and 24.0 $\sigma_\theta$ between 20°N and 15°S (with depth varying between 40 and 80 m), the diapycnal diffusivity values are 0.6 cm$^2$ s$^{-1}$. Farther poleward and deepening, the mixing rate decreases to 0.3 cm$^2$ s$^{-1}$ for 24.5 $\sigma_\theta$ between 30°N and 20°S (depth ~100 m) and to 0.2 cm$^2$ s$^{-1}$ for 25.0 $\sigma_\theta$ between 30°N and 35°S (depth ~120 m). For 25.5 $\sigma_\theta$ between 50°N and 40°S (~150 m), using air–sea flux only results in a diapycnal diffusivity of −0.06 cm$^2$ s$^{-1}$; adding the runoff increases the diffusivity to 0.0 cm$^2$ s$^{-1}$ (Table 4). Zero and negative diffusivity values are physically problematic. We suspect that the near-zero diffusivity values result from the errors in the air–sea heat and freshwater fluxes. Although the actual errors in the air–sea fluxes are unknown from the dataset used in this study, it is most likely that the near-zero net surface fluxes are within their uncertainties. Therefore the resulting near-zero diffusivity values also have no significance. In fact, for even higher latitudes, a global buoyancy budget for water between about 65°N and Antarctica and bounded by isopycnal 27.5 $\sigma_\theta$ (depth ~400 m) yields a diapycnal diffusivity of 0.2 cm$^2$ s$^{-1}$ (Table 3).

## 7. Discussions and conclusions

Diapycnal diffusivity values for the upper oceans were calculated using surface buoyancy fluxes in an effort to determine geographical variations in mixing strength. Because the calculation requires closed isopycnals, it is mainly restricted to shallow surfaces. Only an average value for the whole surface can be obtained. In the previous sections we have interpreted the net buoyancy (heat) export out of the water volume mainly by diapycnal diffusion through the bottom of the isopycnal. This needs some justification since the calculations were mainly done in the upper thermocline and part of the water volumes were in the mixed layer. The role of horizontal eddy flux through the vertical section (mixed layer) of the bounding isopycnal needs to be clarified.

The mixed layer depth ($D$) is highly variable in both time and space. In the north Indian Ocean (say, north of 15°S), both the monthly mean Levitus et al. (1994) atlas and the monthly maps of Rao et al. (1989) show that $D$ varies between 30 and 80 m, with smallest values in May and June and largest values in December and January. However, at higher latitudes, stratification is weak and the mixed layer depth depends more strongly on the specific criterion. Using a 1°C temperature dif-

TABLE 4. Diapycnal diffusivity in the Atlantic Ocean. The values of $K$ outside the parentheses are from air–sea buoyancy flux only, while those in the parentheses include the effect of river runoff.

| $\sigma_\theta$ | Principal location | Approximate depth (m) | Density flux ($10^7$ kg s$^{-1}$) | Surface area ($10^{13}$ m$^2$) | $-d\rho/dz$ ($10^{-2}$ kg m$^{-4}$) | $K_\rho$ (cm$^2$ s$^{-1}$) |
|---|---|---|---|---|---|---|
| 23.0 | E Tropical Atlantic | 30 | −1.47 | 0.37 | 6.3 | 0.6 (0.6) |
| 23.0 | W Tropical Atlantic | 30 | −0.08 | 0.24 | 6.9 | 0.05 (0.4) |
| 23.5 | 20°N–10°S | 45 | −2.60 | 1.43 | 3.7 | 0.5 (0.6) |
| 24.0 | 20°N–15°S | 80 | −2.88 | 2.07 | 3.2 | 0.5 (0.6) |
| 24.5 | 30°N–20°S | 100 | −2.30 | 2.57 | 3.3 | 0.3 (0.3) |
| 25.0 | 30°N–35°S and N Atlantic coast | 120 | −1.34 | 3.63 | 2.7 | 0.10 (0.2) |
| 25.5 | 50°N–40°S | 150 | 0.73 | 5.00 | 2.4 | −0.06 (0.0) |

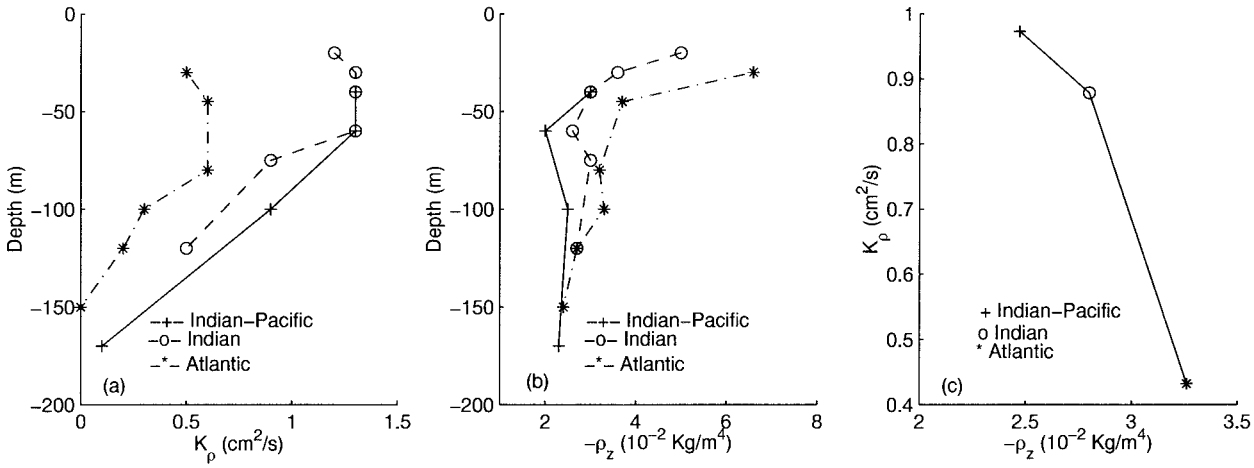


FIG. 11. (a) Average diapycnal diffusivity vs average depth of the isopycnals for the three oceans. Values are taken from Tables 1, 3, and 4. (b) Same as (a) but for average diapycnal density gradient over the isopycnals. (c) Vertically averaged diapycnal diffusivity vs vertically averaged diapycnal density gradient for the three oceans. See text for definition.

ference, the monthly mixed layer depths of Rao et al. (1989) showed that at about 30°S, $D$ varies between 40 (December and January) and 150 m (August and September).

The horizontal eddy flux through the mixed layer portion of a bounding isopycnal can be parameterized as $K_H\overline{\partial\rho/\partial y^*}\cdot L\cdot D$, where $L$ is the lateral length of the bounding isopycnal across the ocean and in the mixed layer, and $\overline{\partial\rho/\partial y^*}$ is the averaged lateral density gradient normal to the bounding surface in the mixed layer. With a ''typical'' value of the horizontal diffusivity $K_H$ ($1 \times 10^7$ cm$^2$ s$^{-1}$), the horizontal eddy fluxes computed from the datasets used in this work are two small to balance the air–sea fluxes. An example is shown in the Indian Ocean for isopycnal 25.0 $\sigma_\theta$ (Fig. 4b), for which $L = 0.9 \times 10^7$ m at about 35°S and $\overline{\rho_y} = -1.3 \times 10^{-6}$ kg m$^{-4}$ from the Levitus et al. (1994) atlas. With a maximum mixed layer depth of 150 m (Rao et al. 1989), the horizontal eddy flux is $0.18 \times 10^7$ kg s$^{-1}$ for $K_H = 1 \times 10^7$ cm$^2$ s$^{-1}$, which is too small to balance the buoyancy gain through the air–sea surface ($4.27 \times 10^7$ kg s$^{-1}$ Table 1). From a different point of view, taking a diapycnal diffusivity ($K_\rho$) value of 0.1 cm$^2$ s$^{-1}$ (as indicated by microstructure and tracer release studies for the ocean interior), the diapycnal diffusive flux through the bottom of isopycnal 25.0 $\sigma_\theta$ would be $K_\rho\overline{\rho_z}A_\rho = -1.0 \times 10^7$ kg s$^{-1}$ (Table 1), which is about one-fourth of the air–sea flux ($-4.27 \times 10^7$ kg s$^{-1}$). If the offset between the above two terms ($-3.27 \times 10^7$ kg s$^{-1}$) is diffused out through the mixed layer section, this would require an average horizontal diffusivity value of $5.6 \times 10^8$ cm$^2$ s$^{-1}$ for a mixed layer depth of 50 m and $1.9 \times 10^8$ cm$^2$ s$^{-1}$ for a mixed layer depth of 150 m. These values are at least one order larger than the values normally cited.

The above results indicate that our near-surface diapycnal diffusivity values (0.5–1.3 cm$^2$ s$^{-1}$) for the Indian Ocean are reasonable. The bottom depths of the annual-mean isopycnals discussed for the Indian Ocean (Figs. 1 and 6) vary between 20 and 150 m, which are in the same depth range as the winter mixed layers (Rao et al. 1989) and intersect the equatorial undercurrent. Intense turbulence supporting strong mixing is observed in such regions (Hebert et al. 1991; Chereskin et al. 1986). For all oceans, our diapycnal diffusivity values decrease rapidly with increasing average isopycnal depth (Tables 1, 3, and 4). The plot of $K_\rho$ versus the mean isopycnal depth (Fig. 11a) shows that $K_\rho$ is relatively constant above 80 m for the Atlantic and 60 m for the Indian–Pacific Ocean. Below that depth, $K_\rho$ decreases rapidly to the values found in the microstructure and tracer studies [$O$(0.1 cm$^2$ s$^{-1}$)]. Differences in $K_\rho(z)$ in the three different oceans (Fig. 11a) are related to the differing stratification (Fig. 11b) and to the geographical location of the isopycnals as this affect the area for averaging (Fig. 10). The larger the stratification, the smaller the diffusivity. This relation is quantitatively shown in Fig. 11c, which displays the vertically averaged diffusivity values versus the vertically averaged stratification values for the three profiles in Figs. 11a and 11b and in the common depth range 40–120 m. Roughly, Fig. 11c shows that $K_\rho$ is inversely proportional to the stratification or the Brunt–Väisälä frequency $N^2$, but the data points are too few to define a quantitative relationship.

One shortcoming of this work is the lack of error estimates for the calculated diffusivity values. A complete error analysis should include errors associated with instrumentation, observational bias (both in time and space/ship tracks), and the objective analysis. Unfortunately, error estimates for the net heat/buoyancy fluxes are not available for the dataset used in this work (A. M. da Silva 1997, personal communication). Only biases for wind and air temperature are available (da Silva et al. 1994). A complete error analysis requires analyz-

TABLE 5. The rms or norm for the annual-mean net heat fluxes (RMSnetheat) and for the standard deviations (RMSstd) of the annual means in the global latitude bands defined in column 1. The annual means and the stds for the annual means are computed from the monthly means. The last column in the table is the ratio of the third column over the second column.

| Latitude band | RMSnetheat (W m$^{-2}$) | RMSstd (W m$^{-2}$) | Ratio |
|---|---|---|---|
| 10°S–10°N | 42.8 | 9.2 | 0.22 |
| 20°S–20°N | 35.6 | 17.4 | 0.49 |
| 40°S–40°N | 38.5 | 30.3 | 0.79 |

ing the raw data and is beyond the scope of this paper. The standard deviations for the annual means, which were calculated from the monthly means, are not a proper representation of the errors for the annual means but rather indications of seasonal variations. These are presented in Table 5 as a reference. In Table 5, the rms values or norms for the annual mean net heat flux and the standard deviations for the annul means are defined as

$$\text{RMSnetheat} = \left[\sum_{i,j} \text{netheat}(i, j)^2/N\right]^{1/2},$$

where the sum is over the $N$ grid points in the latitude bands listed in column 1 for the global ocean. As the zonal band expands from the equator poleward, the relative importance of the standard deviation associated with seasonal variation increases, from about 20% within 10°S and N to about 50% within 20°S and N, and to about 80% within 40°S and N (Table 5, last column). It should be reminded that the eddy flux and eddy diffusivity in this paper are relative to the annual means, as defined in section 2. If a seasonal signal can be resolved from a dataset, as being dealt separately, the values of the eddy flux and eddy diffusivity might vary accordingly.

In conclusion, the estimated average diapycnal diffusivity values for the upper ocean (above 200 m) range from 1.3 to 0.1 cm$^2$ s$^{-1}$. They are larger near the equator and the surface and generally decrease with depth and poleward. In most cases the dependence on depth and on latitude cannot be distinguished for the cases considered since deeper isopycnals also outcrop at higher latitudes. One exception is perhaps the Bay of Bengal and the northeast Indian Ocean. The diapycnal diffusivity values there remain at about 1.3 cm$^2$ s$^{-1}$ for several isopycnals. As the isopycnals deepen, their outcrop lines extend equatorward from the northeast. If one assumes that diapycnal diffusivity is smaller at greater depths (cf. Fig. 11), the constant diffusivity values in this region can only be explained by stronger mixing in the equatorial region. As isopycnals cross the equator and extend farther southward (poleward) and deeper, the diapycnal diffusivity decreases monotonically from 0.9 cm$^2$ s$^{-1}$ for 23.0 $\sigma_\theta$ (north of 20°S) to 0.5 cm$^2$ s$^{-1}$ for 25.0 $\sigma_\theta$ (north of 35°S).

A parallel calculation for isotherms shows larger diathermal diffusivities in the Tropics and smaller ones poleward and with depth. One difficulty in interpreting the larger diathermal diffusivity in the Tropics as stronger diapycnal mixing is that isotherms do not follow isopycnals closely there, and the much larger isopycnal diffusivity might have a component in the diathermal direction.

For the water bounded by isopycnal 25.0 $\sigma_\theta$, the buoyancy budget yields a diapycnal diffusivity of 0.5 cm$^2$ s$^{-1}$ for the Indian Ocean and of 0.1 cm$^2$ s$^{-1}$ for the Indian–Pacific system. The Atlantic Ocean diffusivity (0.2 cm$^2$ s$^{-1}$) is smaller than in the Indian Ocean, likely because this isopycnal extends farther poleward in the Atlantic than in the Indian Ocean. (The average isopycnal depths are similar.) The Atlantic diffusivity is larger than that in the Indian–Pacific system, likely because this isopycnal is shallower in the Atlantic than in the Pacific. The Amazon runoff significantly affects the buoyancy budget in the western tropical Atlantic, where diapycnal diffusivity for 23.0 $\sigma_\theta$ ($\sim$30 m) is 0.05 cm$^2$ s$^{-1}$ without the runoff and 0.4 cm$^2$ s$^{-1}$ with the runoff.

The diapycnal diffusivity values presented here are consistent with the previously reported values and with prior findings that mixing is stronger in boundary/surface regions and near the equator than in the quiet ocean interior. The tracer release experiments in NATRE (e.g., Ledwell at al. 1993) indicated that diapycnal mixing is slow in the open ocean: the diapycnal diffusivity averaged over hundreds of kilometers and five months was 0.11 ($\pm$0.02) cm$^2$ s$^{-1}$ near 300-m depth. In the same experiment (NATRE), Sherman and Davis (1995) estimated a diapycnal diffusivity of 0.14 cm$^2$ s$^{-1}$ using 76 profiles of temperature microstructure between 200-m and 350-m depth over a ten-day period. These values are similar to open-ocean values inferred from dissipation-flux treatment of microstructure measurements in the upper kilometers (Gregg 1987, 1989; Gregg and Sanford 1988; Moum and Osborn 1986). Profiles of diapycnal eddy diffusivity to a maximum depth of 4000 m were derived from ocean velocity and temperature microstructure data in the northeast Pacific and northeast Atlantic oceans by Toole et al. (1994) and recently in the Brazil Basin of the South Atlantic by the same group (Polzin et al. 1997). They found that in the ocean interior where the internal wave field is at background intensity, the diapycnal eddy diffusivity was small (on the order of 0.1 cm$^2$ s$^{-1}$ or even smaller); enhanced dissipation was observed in regions of elevated internal wave energy, particularly near steeply sloping boundaries (where the eddy diffusivity estimates exceed 1 cm$^2$ s$^{-1}$). Enhanced mixing in boundary regions was estimated from passive tracers in the Santa Monica and Santa Cruz Basins (Ledwell et al. 1995). Strong bottom mixing was also found from water mass and heat budgets for various basins: 3–4 cm$^2$ s$^{-1}$ for the deep Brazil Basin (Hogg et al. 1982), 1–4 cm$^2$ s$^{-1}$ for various depths in the deep western North Atlantic (Whitehead and Worthington

1982), and 4 $cm^2\ s^{-1}$ for the North Atlantic at 2°C (Luyten et al. 1993). Extraordinarily high rates of mixing were found in the deep Samoan passage and adjacent regions (Roemmich et al. 1996). Hebert et al. (1991) and Moum et al. (1992) found that turbulence was enhanced above the equatorial undercurrent in comparison to latitudes north and south of it. In a layered model of a steady geostrophic ocean, de Szoeke (1995) argued that it is necessary to have far larger diapycnal diffusivities than $O(1\ cm^2\ s^{-1})$ to accomplish meridional buoyancy transports. These results suggest that basin-averaged mixing rates may be dominated by intensive processes occurring locally (e.g., near the ocean boundaries). The diffusivity values cited above covers a large spectrum, corresponding to the different regimes in physics and in space. We hope that the estimates presented in this paper fill some gaps in the mixing rate spectrum.

*Acknowledgments.* Encouraging discussions with R.-X. Huang are greatly appreciated. We thank M. Morris for providing the XBT data and A. da Silva for the air–sea flux data through the Web site atlas. We thank D. Cayan for discussions on the NASA MSU precipitation and T. Rossby for his careful reading of and comments on the manuscript. Critics and suggestions by J. Toole, N. Hogg, and an anonymous reviewer greatly improved the presentation of this work. This work was supported by the NOAA JIMO postdoctoral fellowship and by the Vetlesen Foundation.

## REFERENCES

Baumgartner, A., and E. Reichel, 1975: *The World Water Balance.* Elsevier, 179 pp.

Chereskin, T. K., J. N. Moum, P. J. Stabeno, D. R. Caldwell, L. A. Regier, and D. Halpern, 1986: Fine-scale variability at 140 degrees W in the equatorial Pacific. *J. Geophys. Res.,* **91,** 12 887–12 897.

da Silva, A. M., C. C. Young, and S. Levitus, 1994: *Atlas of Surface Marine Data 1994.* Vol. 3: *Anomalies of Heat and Momentum Fluxes*; Vol. 4: *Anomalies of Fresh Water Fluxes* NOAA Atlas NESDIS 8, U.S. Department of Commerce, NOAA, NESDIS, 413 pp.

de Szoeke, R. A., 1995: A model of wind- and buoyancy-driven ocean circulation. *J. Phys. Oceanogr.,* **25,** 918–941.

Duda, T. F., and D. C. Jacobs, 1995: Comparison of shear measurements and mixing predictions with a direct observation of diapycnal mixing in the Atlantic thermocline. *J. Geophys. Res.,* **100,** 13 481–13 498.

Eriksen, C. C., 1985: Implications of ocean bottom reflection for internal wave spectra and mixing. *J. Phys. Oceanogr.,* **15,** 1145–1156.

Fu, L.-L., 1986: Mass, heat and freshwater fluxes in the South Indian Ocean. *J. Phys. Oceanogr.,* **16,** 1683–1693.

Gargett, A. E., 1990: Do we really know how to scale the turbulent kinetic energy dissipation rate due to breaking of oceanic internal waves? *J. Geophys. Res.,* **95,** 15 971–15 974.

——, and G. Holloway, 1992: Sensitivity of the GFDL ocean model to different diffusivities for heat and salt. *J. Phys. Oceanogr.,* **22,** 1158–1177.

Garrett, C., K. Speer, and E. Tragou, 1995: The relationship between water mass formation and the surface buoyancy flux, with application to Phillips' Red Sea model. *J. Phys. Oceanogr.,* **25,** 1696–1705.

Gregg, M. C., 1987: Diapycnal mixing in the thermocline: A review. *J. Geophys. Res.,* **92,** 5249–5286.

——, 1989: Scaling the turbulent dissipation in the thermocline. *J. Geophys. Res.,* **94,** 9686–9698.

——, and T. B. Sanford, 1988: The dependence of turbulent dissipation on stratification in a diffusively stable thermocline. *J. Geophys. Res.,* **93,** 12 381–12 392.

——, and E. Kunze, 1991: Shear and strain in Santa Monica Basin. *J. Geophys. Res.,* **96,** 16 709–16 719.

Hastenrath, S., and P. Lamb, 1980: On the heat budget of hydrosphere and atmosphere in the Indian Ocean. *J. Phys. Oceanogr.,* **10,** 694–708.

Hebert, D., J. N. Moum, and D. R. Caldwell, 1991: Does ocean turbulence peak at the equator?: Revisited. *J. Phys. Oceanogr.,* **21,** 1690–1698.

Hogg, N., 1987: A least-squares fit of the advective–diffusive equations to Levitus atlas. *J. Mar. Res.,* **45,** 347–375.

——, P. Biscaye, W. Gardner, and W. J. Schmitz Jr., 1982: On the transport and modification of Antarctic Bottom Water in the Vema Channel. *J. Mar. Res.,* **40,** 231–263.

Hsiung, J., 1985: Estimates of global oceanic meridional heat transport. *J. Phys. Oceanogr.,* **15,** 1405–1413.

Ledwell, J. R., and A. Bratkovich, 1995: A tracer study of mixing in the Santa Cruz Basin. *J. Geophys. Res.,* **100,** 20 681–20 704.

——, and B. M. Hickey, 1995: Evidence for enhanced boundary mixing in the Santa Monica Basin. *J. Geophys. Res.,* **100,** 20 665–20 679.

——, A. J. Watson, and C. S. Law, 1993: Evidence for slow mixing across the pycnocline from an open-ocean tracer-release experiment. *Nature,* **364,** 701–703.

Lee, T., and J. Marotzke, 1997: Inferring meridional mass and heat transports of the Indian Ocean by fitting a general circulation model to climatological data. *J. Geophys. Res.,* **102,** 10 585–10 602.

Levitus, S., and T. Boyer, 1994: *World Ocean Atlas 1994.* Vol. 4: *Temperature.* NOAA, Atlas NESDIS 4. U.S. Department of Commerce, NOAA, NESDIS, Washington, D.C., 117 pp.

——, R. Burgett, and T. Boyer, 1994: *World Ocean Atlas 1994.* Vol. 3: *Salinity.* NOAA, Atlas NESDIS 3. U.S. Department of Commerce, NOAA, NESDIS, Washington, D.C., 99 pp.

Lukas, R., T. Yamagata, and J. P. McCreary, 1996: Pacific low-latitude western boundary currents and the Indonesian through flow. *J. Geophys. Res.,* **101,** 12 209–12 216.

Luyten, J., M. McCartney, H. Stommel, R. Dickson, and E. Gmitrowicz, 1993: On the sources of North Atlantic Deep Water. *J. Phys. Oceanogr.,* **23,** 1885–1892.

Macdonald, A., 1995: Oceanic fluxes of mass, heat, and freshwater: a global estimate and perspective. Ph.D. dissertation, MIT/WHOI, 326 pp.

McDougall, T. J., 1987: Neutral surfaces. *J. Phys. Oceanogr.,* **17,** 1950–1964.

McWilliams, J. C., G. Danabasoglu, and P. R. Gent, 1996: Tracer budgets in the warm water sphere. *Tellus,* **48A,** 179–192.

Meyers, G., R. Bailey, and A. Worby, 1995: Geostrophic transport of Indonesian through-flow. *Deep-Sea Res.,* **42,** 1163–1174.

Montgomery, R. B., 1938: Circulation in the upper layers of southern North Atlantic deduced with use of isentropic analysis. *Paps. Phys. Oceanogr. Meterol.,* **6** (2), 1–55.

Morris, M. Y., 1996: Mean and low frequency fluctuations in the circulation of the western/central Pacific Ocean. Ph.D. dissertation, University of California, San Diego, 203 pp.

Moum, J. N., and T. R. Osborn, 1986: Mixing in the main thermocline. *J. Phys. Oceanogr.,* **16,** 1250–1259.

——, D. Hebert, C. A. Paulson, and D. R. Caldwell, 1992: Turbulence and internal waves at the equator. Part I: Statistics from towed thermistors and a microstructure profiler. *J. Phys. Oceanogr.,* **22,** 1330–1345.

Munk, W. H., 1966: Abyssal recipes. *Deep-Sea Res.,* **13,** 707–730.

Niiler, P. P., and J. Stevenson, 1982: On the heat budget of tropical warm water pools. *J. Mar. Res.,* **40** (Suppl.), 465–480.

Oberhuber, J., 1988: *An Atlas Based on the COADS Data Set: The Budgets of Heat, Buoyancy, and Turbulent Kinetic Energy at the Surface of the Global Ocean.* Report No. 15, Max-Planck-Institut für Meteoroloie, 199 pp.

Olbers, D. J., M. Wenzel, and J. Willebrand, 1985: The inference of North Atlantic circulation patterns from climatological hydrographic data. *Rev. Geophys.,* **23,** 313–356.

Polzin, K. L., J. M. Toole, and R. W. Schmitt, 1995: Finescale parameterizations of turbulent dissipation. *J. Phys. Oceanogr.,* **25,** 306–328.

——, ——, J. R. Ledwell, and R. W. Schmitt, 1997: Spatial variability of turbulent mixing in the abyssal ocean. *Science,* **276,** 93–96.

Rao, R. R., R. L. Molinari, and J. F. Festa, 1989: Evolution of the climatological near-surface thermal structure of the tropical Indian Ocean: 1. Description of mean monthly mixed layer depth, and sea surface temperature, surface current, and surface meteorological fields. *J. Geophys. Res.,* **94,** 10 801–10 815.

Robbins, P. E., and J. M. Toole, 1996: The dissolved silica budget as a constraint on the meridional overturning circulation of the Indian Ocean. *Deep-Sea Res.,* **44,** 879–906.

Roemmich, D., S. Hautala, and D. Rudnick, 1996: Northward abyssal transport through the Samoan passage and adjacent regions. *J. Geophys. Res.,* **101,** 14 039–14 055.

Semtner, A., Jr, and R. Chervin, 1992: Ocean general circulation from a global eddy-resolving model. *J. Geophys. Res.,* **97,** 5493–5550.

Sherman, J. T., and R. E. Davis, 1995: Observations of temperature microstructure in NATRE. *J. Phys. Oceanogr.,* **25,** 1913–1929.

Slutz, R., S. Lubker, J. Hiscox, S. Woodruff, R. Jenne, D. Joseph, P. Steurer, and J. Elms, 1985: *COADS, Comprehensive Ocean–Atmosphere Data Set,* Release 1. Climate Research Program, Environmental Research Laboratory, 262 pp.

Speer, K. G., and E. Tziperman, 1992: Rates of water mass formation in the North Atlantic Ocean. *J. Phys. Oceanogr.,* **22,** 93–104.

——, H. J. Isemer, and A. Biastoch, 1995: Water mass formation from revised COADS Data. *J. Phys. Oceanogr.,* **25,** 2444–2457.

Spencer, R., 1993: Global oceanic precipitation from the MSU during 1979–91 and comparisons to other climatologies. *J. Climate,* **6,** 1301–1326.

Spitzer, W. S., and W. J. Jenkins, 1989: Rates of vertical mixing, gas exchange and new production: Estimates from seasonal gas cycles in the upper ocean near Bermuda. *J. Mar. Res.,* **47,** 169–196.

Stommel, H., and A. B. Arons, 1960: On the abyssal circulation of the world ocean-I. Stationary planetary flows on a sphere. *Deep-Sea Res.,* **6,** 140–154.

Stricherz, J., D. M. Legler, and J. J. O'Brien, 1992: *Atlas of Florida State University Indian Ocean Winds for TOGA 1970–1985.* The Florida State University, 250 pp.

Toole, J. M., and M. Raymer, 1985: Heat and fresh water budgets of the Indian Ocean—Revisited. *Deep-Sea Res.,* **32,** 917–928.

——, and B. A. Warren, 1993: A hydrographic section across the subtropical South Indian Ocean. *Deep-Sea Res.,* **40,** 1973–2019.

——, K. L. Polzin, and R. W. Schmitt, 1994: Estimates of diapycnal mixing in the abyssal ocean. *Science,* **264,** 1120–1123.

Tziperman, E., 1986: On the role of interior mixing and air-sea fluxes in determining the stratification and circulation of the oceans. *J. Phys. Oceanogr.,* **16,** 680–693.

UNESCO, 1978: *World Water Balance and Water Resources of the Earth.* UNESCO, Paris, 663 pp.

——, 1969–1992: *Discharge of Selected Rivers of the World*: Vol.1, 1969; Vol.2, 1971; Vol.3, Parts 1–5, 1969–1992.

Walin, G., 1982: On the relation between sea-surface heat flow and thermal circulation in the ocean. *Tellus,* **34,** 187–195.

Warren, B., 1994: Driving the meridional overturning in the Indian Ocean. *Deep-Sea Res.,* **41,** 1349–1360.

Welander, P., 1971: The thermocline problem. *Philos. Trans. Roy. Soc. London,* **A270,** 415–442.

Whitehead, J. A., and L. V. Worthington, 1982: The flux and mixing rates of Antarctic Bottom Water within the North Atlantic. *J. Geophys. Res.,* **87,** 7903–7924.

Wijffels, S. E., R. W. Schmitt, and H. L. Bryden, 1992: Transport of freshwater by the oceans. *J. Phys. Oceanogr.,* **22,** 155–162.

Zhang, H., and N. Hogg, 1992: Circulation and water mass balance in the Brazil Basin. *J. Mar. Res.,* **50,** 385–420.